buckling building codes columns continuous

girder bridge durability dynamic analysis

dynamic response earthquake

finite element analysis finite element

method meridional stresses operational

modal analysis optimization reinforced

concrete seismic analysis seismic

design seismic isolation seismic response

shallow foundations smart concrete

teaching-learning based optimization

TULPAR
ACADEMIC PUBLISHING

Challenge Journal
OF STRUCTURAL MECHANICS

CONTENTS

Research Articles

Reviews

TULPAR
ACADEMIC PUBLISHING

Research Article

Effects of structural irregularities on low and mid-rise RC building response

Hüseyin Bilgin *, Rezarta Uruçi

Department of Civil Engineering, Epoka University, 1032 Tirana, Albania

ABSTRACT

During the recent earthquakes, it has been observed that structural irregularities are one of the main reasons of the building damage. Irregularities are weak points in a building which may cause failure of one element or total collapse of the building during an earthquake. Since Albania is a country with moderate seismicity which has been hit by earthquakes of different magnitudes many times establishes the need to study the effect of irregularities is well-founded. The main structural irregularities encountered in Albanian construction practice consist of short column, large and heavy overhangs and soft story. In this study, these types of irregularities are considered in two different types of buildings, low and mid-rise reinforced concrete frame buildings represented by 3- and 6- story respectively. Pushover analyses are deployed to get the effect of structural irregularities on RC building response. A building set is chosen to represent the existing construction practice in the region; regular framed building and buildings with irregularities such as soft stories, short columns, heavy overhangs and the presence of soft story with heavy overhangs. The analyses have been conducted by using ETABS and Seismosoft software. Pushover curves of building set are determined by nonlinear static analysis in two orthogonal directions. Comparative performance evaluations are done by considering EC8 and Albanian Seismic codes (KTP-N2-89). From the obtained results, it is observed that low and mid-rise structures with soft story- two sided overhangs and short column are more vulnerable during earthquakes.

1. Introduction

The inadequate performance and the huge number of collapsed buildings during past earthquakes due to different structural irregularities determines the idea to analyze the buildings with dissimilar irregularities in order to understand the effect of irregularities on reinforced concrete (RC) buildings under seismic effects (Varadharajan, 2014; Altuntop, 2007; Dolsek and Fajfar, 2000; Inel and Ozmen, 2008; Uruci and Bilgin, 2016; Sattar and Liel, 2010; Apostolska et al., 2010; Sonmez, 2013; Vahidi and Malekabadi, 2009; Tena-Colunga, 2004). Structural irregularities have a significant effect on the response of RC buildings during an earthquake. In order to prevent possible damages caused by structural irregularities, seismic demand must be determined accurately. Several researchers and academicians (Varadharajan, 2014; Altuntop, 2007), have studied altered vertical and horizontal irregularities with different methods of analysis such: nonlinear static pushover analysis and time history analysis, etc. and realized which type of irregularities are riskier during an earthquake and what should be taken in consideration during the design process (Bachmann, 2002; Semnani et al., 2014). Albanian building stock is mostly composed of RC and masonry buildings. Most of these buildings are designed according to earlier versions of Albanian Seismic Codes (KTP-

N2-89, 1989) and some of them were constructed without a definite construction project. Considering these facts and the observations done in Albanian construction industry, presence of structural irregularities is very common in these buildings. The aim of this study is to evaluate the seismic performance of 3- and 6- story RC buildings representing the low and mid-rise building stock of Albanian construction practice, in which soft story, short column and heavy overhangs irregularities are imposed, in order to evaluate the effects of structural irregularities on RC frame structure response. Effect of structural irregularities and performance of the considered frames are assessed by using capacity curves of the frames.

2. Case Study

2.1. Description of the building set

Two different 3- and 6- story RC structures are considered to represent reference low and mid-rise buildings in the region in this study. The selected buildings are typical RC frame buildings with no shear walls. Selected buildings have the same plan view, 20m by 16 m in plan. Both have 5 bays by 4m along *x* direction and 4 bays by 4m along *y* direction as shown in Figs. 1-2. Typical floor height for both frames is 3m. The location of masonry infill walls in plan is shown by the hatch of beams for both structures, Figs. 1-2.
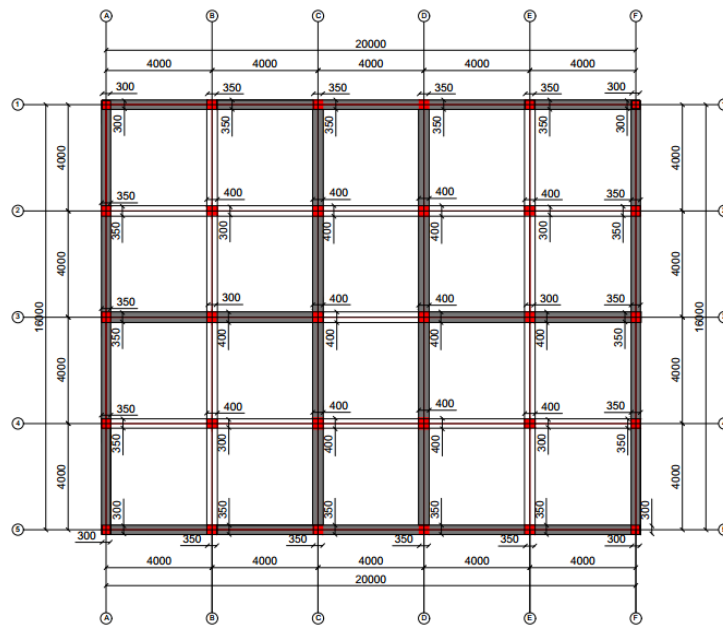
Fig. 1. Structural plan view of the 3-story frame (units in mm).
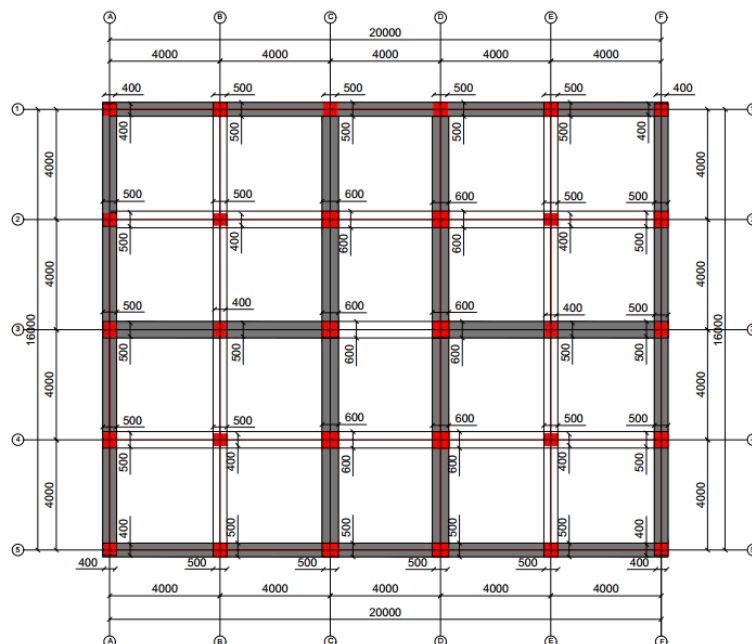
Fig. 2. Structural plan view of the 6-story frame (units in mm).

Beam and column dimensions of the reference buildings represent the most common frame elements for low and mid-rise frames in Albanian construction practice. The 3- story frame consists of 300mm x 300mm and 350mm x 350mm outside columns, identified as C1 and C2 respectively, 300mm x 400mm, 400mm x 300mm and 400mm x 400 mm inside columns, identified as C5, C4 and C3 respectively, as shown in Figure 3. Beams have all the same section for the 3- story frame which consists of 300mm x 400 mm (Fig. 3). The 6- story frame consists of 400mm x 400mm and 500mm x 500mm outside columns, and 400mm x 500mm, 500mm x 400mm and 400mm x 600 mm inside columns, identified as C9, C8 and C7 respectively, as shown in Figure 4. All the beams of the 6-story frame have the same cross section of 300mm x 500mm Fig. 4. The transverse reinforcement is represented 100mm by spacing in order to reflect the ductile detailing. The selected reference buildings do not have any vertical or horizontal irregularity (short columns, soft story, overhangs, etc.)
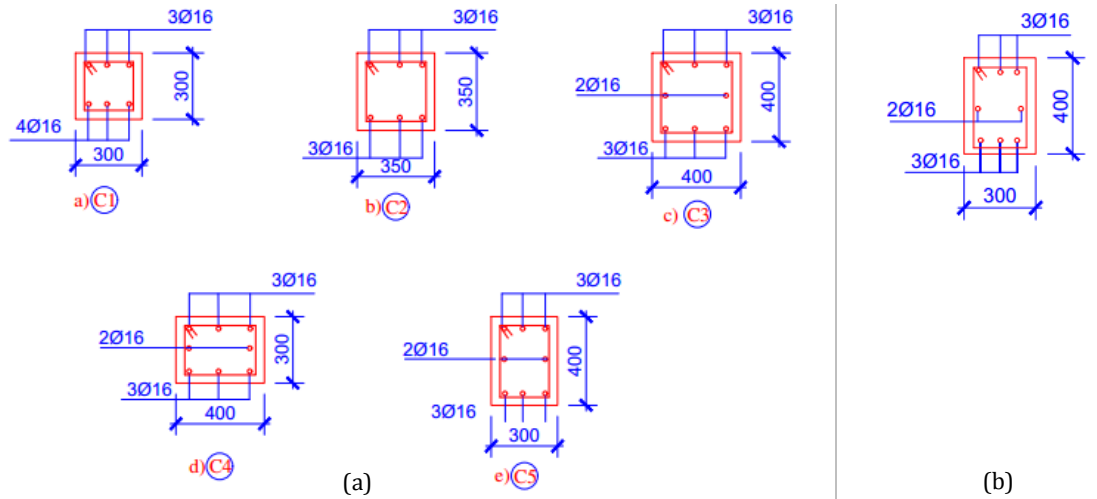
Fig. 3. a) Column and, b) Beam reinforcement details for 3-story frame (units in mm).
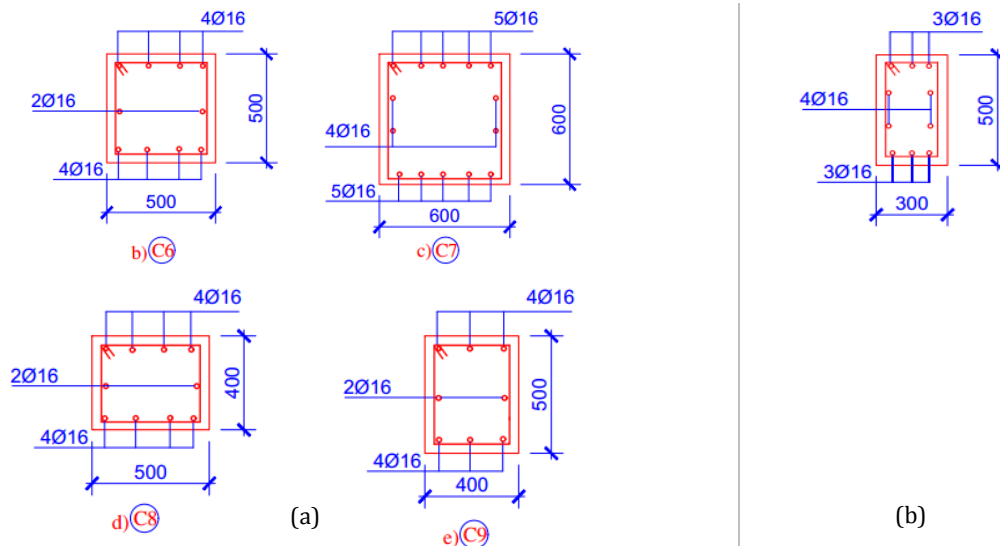
Fig. 4. (a) Column and, (b) Beam reinforcement details for 6-story frame (units in mm).

Soft story in most of the cases happens because of the lower stiffness of the first story of the buildings which comes as a result of fewer amounts of masonry infill walls or because the first story may have greater height compared to the other ones because of commercial reasons (Altuntop, 2007; Dolsek and Fajfar, 2000; Inel and Ozmen, 2008; Uruci and Bilgin, 2016; Sattar and Liel, 2010; Apostolska et al., 2010; Sonmez, 2013). In this study both cases are taken in consideration for the two types of structures, low and mid-rise buildings. In the first story of the selected frames the masonry infill walls are removed, and the story height is done 4.5m instead of 3m normal height, Fig. 5(b). Short column may be formed because of different situations like band windows, mid story beams at the stairway shafts in buildings, semi-infilled frames, etc. (Vahidi and Malekabadi, 2009). In this study, short column is created by semi-infilled frames. As seen in the Fig. 5(d), because of two semi-infilled bays four columns have become short. Heavy overhangs shift the buildings mass centre upwards and

take it away from centre of rigidity. Thus, it has negative effects on seismic behaviour. Past earthquakes revealed that buildings with heavy overhangs are more vulnerable to damage (Tena-Colunga, 2004). In this study are modelled overhangs at two cross sides of a building. For this purpose, 1.5m overhangs are attached to the regular building sides Fig. 5(c). The wall loadings are shuffled on the beams nearby the overhang portion. All the building set with different configurations are shown in Table 1.
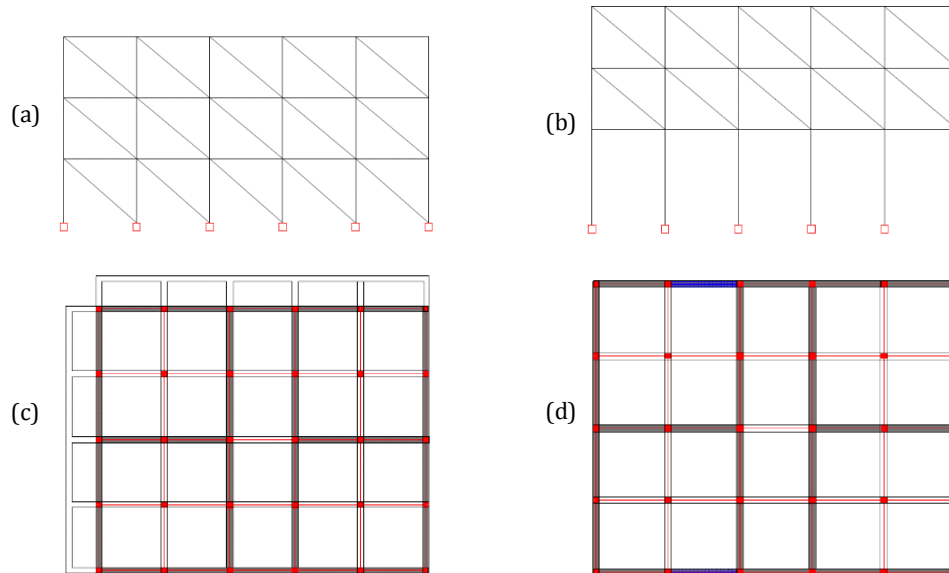
Fig. 5. (a) Reference frame; (b) Soft story; (c) Two-sided overhang; (d) Short column.

Table 1. Building set (3- and 6- story frames).

Ref	Reference Building (without any irregularity), Figure 5(a).
TSO	Two-sided overhang building, Fig. 5(c).
SSH	Soft story due to 4.5 m ground story height (instead of 3 m), Fig. 5(b).
SSW	Soft story due to absence of masonry infill wall at ground story, Fig. 5(b).
SS-H-W	Soft story due to both height and infill effect, Fig. 5(b).
SS-H-W-TSO	Soft story due to both height and infill, and two-sided overhang, Fig. 5(c).
SHC	Short column due to semi-infilled bays at ground story, Fig. 5(d).

* These models are considered for both 3- and 6- story buildings.

2.2. Material properties

Material properties are based on most common materials used in Albanian construction practice; it is assumed 20 MPa for the concrete compressive strength and 355 MPa for the yield strength of reinforcement. Then in order to get the effect of structural irregularities in reinforced concrete structures the selected 3 and 6 story buildings, Fig. 5(a), are modified to have one or more of the above-mentioned structural deficiencies: soft story, short column, overhangs observed in last earthquakes.

2.3. Modeling

Modelling of the considered frames in ETABS is done in similar way for all of them with small changes while implementing the considered structural irregularities. In the below section a step by step analysis is explained for the Ref 3 story frame.

Firstly material and frame sections are defined in accordance with the properties defined in section 2.2. Then the selected frames are modelled by using ETABS software, in Fig. 6 below is shown elevation view of the 'Ref' 3-story reinforced concrete frame.

The model in Fig. 6 is formed by beam and columns whose joints connected to the ground story are made fixed supports in order to be restrained in all directions.

Masonry infill walls include partially of fully panels within the plane of concrete frames, which are bounded by columns and beams. Masonry infill walls are modelled as diagonal strut elements with:

Modulus of elasticity = 1000 MPa
Compressive strength =1 MPa
Shear strength = 0.15 MPa
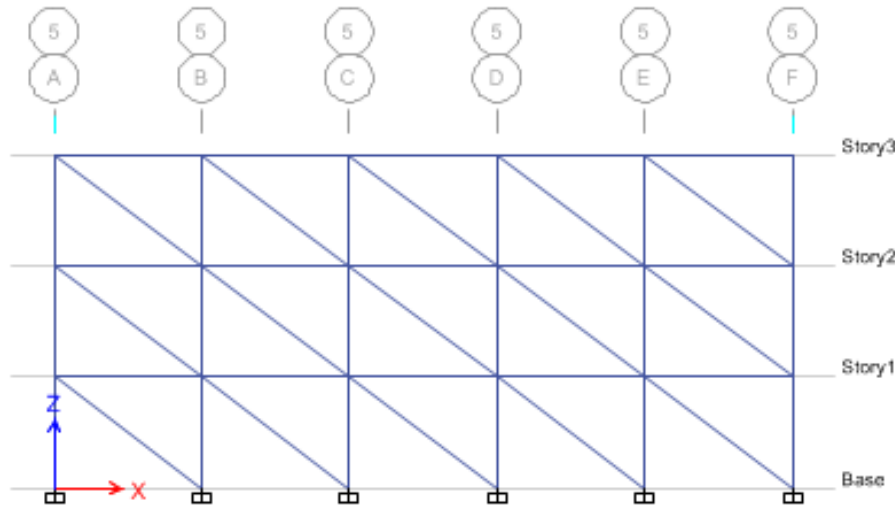
Fig. 6. Elevation view of the Ref 3-story frame.

The elastic stiffness of a masonry infill panel is represented by an equivalent diagonal compression strut with width "*a*" as in Eq. (1) below. The strut have the same thickness and modulus of elasticity as the infill panel it represents:

$$a = 0.175(\lambda_1 \, h_{col})^{-0.4} r_{inf} \, , \qquad (1)$$

where,

$$\lambda_1 = \left[\frac{E_{me} \, t_{inf} \sin 2\theta}{4 E_{fe} \, I_{col} \, h_{inf}} \right]^{\frac{1}{4}} , \qquad (2)$$

h_{inf} = Height of infill panel,
E_{fe} = Expected modulus of elasticity of frame material,
E_{me} = Expected modulus of elasticity of infill material,
I_{col} = Moment of inertia of column,
L_{inf} = Length of infill panel,
r_{inf} = Diagonal length of infill panel,
t_{inf} = Thickness of infill panel and equivalent strut,
θ = Angle whose tangent is the infill height to-length aspect ratio, radians,
λ_1 = Coefficient used to determine equivalent width of infill strut.

In case of non-composite infill panels only the panels in direct contact with frame elements should be taken in consideration while determining the in plane stiffness. In plane lateral stiffness is not the sum of the panel and infill stiffness because of the interaction of the infill with the frame. From the tests it is seen that during an earthquake the infill tends to separate from the frame making possible for the compressive stresses to be created. So masonry infill panels could be represented by a single equivalent strut as shown in Fig. 7, for which if thickness and modulus of elasticity are assumed the same as those of the masonry just width is needed to be determined.

Transfer of forces from one story to another in a masonry infilled frame incorporated with concrete or steel should be considered a deformation-controlled action. Expected shear strength of the in-plane panels should be determined with the Eq. (3) as follows:
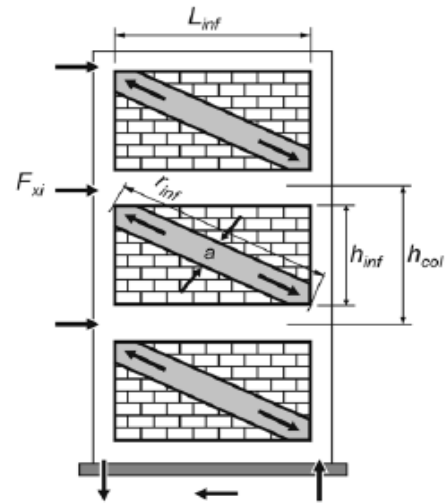
Fig. 7. Masonry infill walls as single equivalent diagonal strut.

$$Q_{CE} = V_{ine} = A_{ni} \, f_{vie} \, , \qquad (3)$$

where,
A_{ni} = Area of net mortared/grouted section across infill panel,
f_{vie} = Expected shear strength of masonry infill.

In Eq. (3), expected shear strength should not exceed the expected masonry bed-joint shear strength.

After modelling the masonry infill walls, load patterns are defined:
• Dead load
• Live load
• Dead load from slabs
• Dead loads of infill walls

Self-weight multiplier of dead loads from infill walls and slabs are taken as 0. Since after the linear analysis the nonlinear analysis is performed and the slabs are not considered in this case for simplicity in calculations, loads are directly assigned as a uniformly distributed loads on beam. After assigning all the considered loads, their combination is done. Two load combinations are

considered: Load combinations in this linear analysis will be two:

• 1.4 DD (dead loads) + 1.6 LL (live loads)
• DL (dead loads) + 0.3 LL (live loads)

After defining the load combinations the linear analysis is carried out. By choosing Modal case, dynamic characteristics of the buildings are obtained for the first 9 first modes.

Nonlinear static pushover analysis is a type of analysis which is performed by subjecting a monotonically increasing pattern of lateral loads in the structure which represents the forces that the structure may experience during an earthquake. Under incrementally increasing loads various structural elements may yield sequentially. Consequently, at each event, the structure experiences a loss in stiffness. Using a pushover analysis, a characteristic non-linear force displacement relationship can be determined. Guidelines like FEMA 356 (2000) have mentioned the modelling procedures, acceptance criteria and analysis procedures for the pushover analysis.

Nonlinear properties of the frame elements are assigned as plastic hinges:

• Beam: Plastic hinges are assigned to the start, 0, and end, 1, point of the beam as specified in FEMA 356. Beams will be released in rotational moment M3.

• Columns: Plastic hinges for columns with have different degree of freedom, axial force and rotational moment in both directions, P-M2-M3.

After assigning the plastic hinges the load cases for the nonlinear static pushover analysis is defined: Firstly the "Push Combo Case" is defined as nonlinear case in which are included the dead loads, dead loads from slabs, infill walls and 30% of live loads. Pushover Analysis is performed in two orthogonal directions. P-Delta effect is taken in consideration. Results are obtained in multiples steps. For the displacement control the maximum displacement at the top of the building is considered. After defining all load cases for the nonlinear analysis, the rigid diaphragms are assigned to each story in order to concentrate the story weight in center of mass.

2.4. Modelling in Seismosoft

Seismosoft is a finite element software used for structural analysis, being able to predict large displacement behaviour of space frames under static or dynamic loadings. The Ref frame is also analysed by Sesimosoft software in order to see the difference between two programs and compare the behaviour of considered reinforced concrete frames.

Firstly material properties and frame sections are defined as shown in Fig. 8 below.
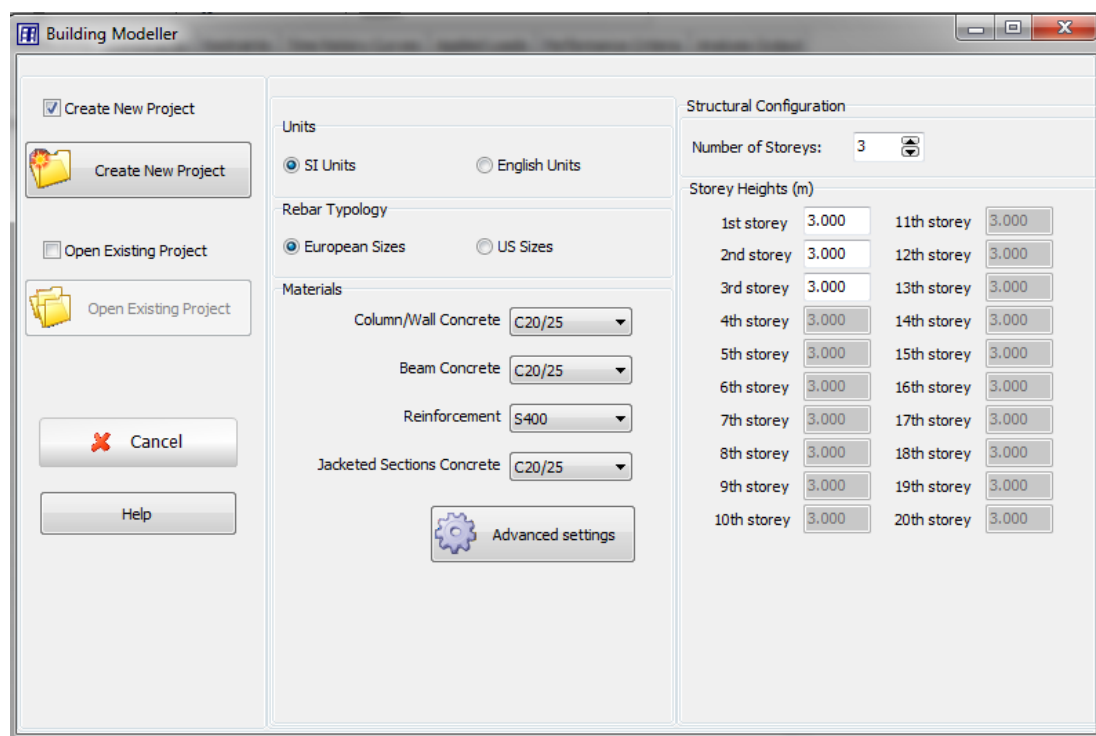
Fig. 8. Defining material properties and frame sections.

After defining the materials, analysis and loading type are chosen, in this case static pushover analysis and uniform distribution respectively. Frame elements are modelled as inelastic plastic hinge force based frame elements. Loading combination factors is 1 for dead loads and 0.3 for live loads. Then the modelling of the Ref frame for the 3 story case is done as shown in Fig. 9.

After modelling the frame elements, masonry infill walls are modelled as diagonal strut elements, in accordance with the structural plan of the 3 story frame where location of masonry infill walls is shown. After modelling of all elements and specifying the loads and pushover analysis parameters the analysis is run out and the results are generated.
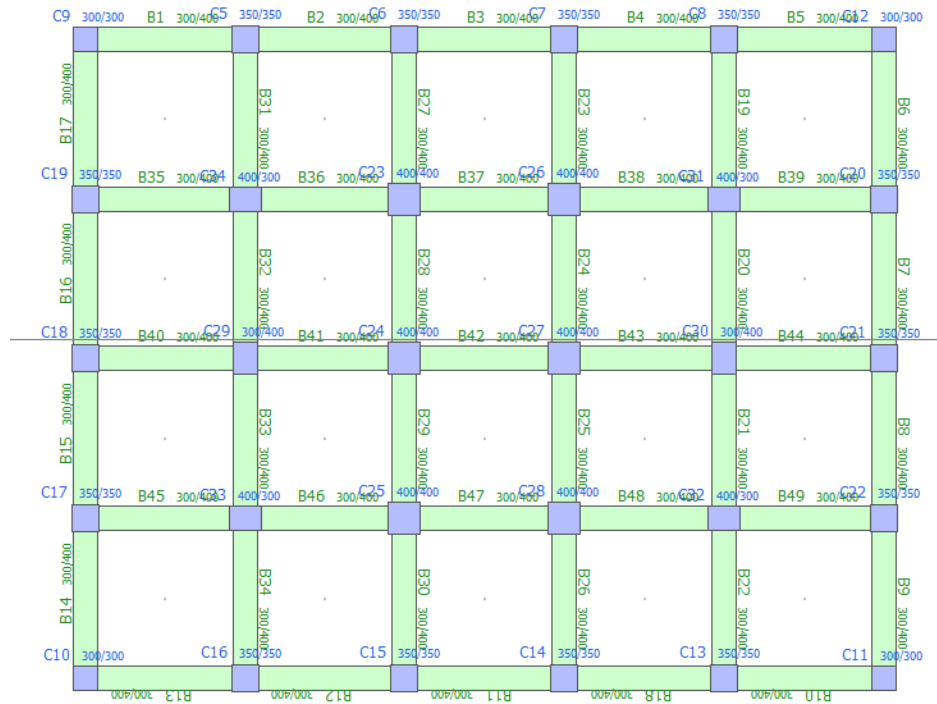
Fig. 9. Plan view of 3 story Ref frame.

3. Structural Analysis

Nonlinear static pushover analysis is a type of analysis which is performed by subjecting a monotonically increasing lateral load patterns in the structure which represents the forces that the structure may experience during an earthquake. Under incrementally increasing loads various structural elements may yield sequentially. Consequently, at each event, the structure experiences a loss in stiffness. Using a pushover analysis, a characteristic non-linear force displacement relationship can be determined. Guidelines like FEMA 356 have mentioned the modelling procedures, acceptance criteria and analysis procedures for the pushover analysis (FEMA-356, 2000). This guideline defines the force-deformation criteria for possible locations of lumped inelastic behavior defined as plastic hinges in the pushover analysis.

In this study, pushover analysis has been conducted for the 14 building models (Table 1) for both type of structures, 3- and 6-story buildings. The material nonlinearities are assigned as plastic hinges; release in rotational moment M3 for flexural hinges for beams and axial force, rotational moment in both directions P-M2-M3 flexural hinges for columns. Infill panels are modelled by one nonlinear strut elements, which only has compressive strength. Then each lateral load pattern is applied and static pushover analyses results of the case study buildings are generated. Behaviour of the structure is represented by capacity curves that represents the base shear force and displacement of the roof. Figs. 10(a-d) illustrates capacity curves obtained from the pushover analysis of the 3 and 6-story frames. In *x*- axis is shown the roof drift ratio that is roof displacement normalized by the building height and in *y*- axis is shown the shear strength coefficient that is the base shear force normalized by the seismic weight.

In the below graphs, Figs. 10(a-d) are shown the normalized graphs of the Ref 3- and 6- story frames, analysed with both software's ETABS and Seismosoft.

From the graphs, it is seen that the programs have generated almost the same capacity curves for both reference frames, 3- and 6- stories. For the rest of the analyses of the other frames are done by using just ETABS software.

In the below graphs, Figs. 11(a-d), are shown the capacity curves of the considered 3- and 6- story regular frames and frames with structural irregularities. From the normalized graphs, presence of structural irregularities effects the seismic performance of the frame, it both weakens and softens the system.

Soft story due to absence of masonry infill walls at the ground story is found to be more damaging than the soft story due to greater height of the ground story in both cases low and mid-rise buildings, 3-and 6-story respectively. Soft story due to absence of infill has shown approximately 33% lower stiffness, 25% lower strength than soft story due to higher story height and 54% lower stiffness, 30% lower strength than the Ref building, for the 3- story frame in x direction. Soft story due to lack of masonry infill walls for the 6- story frame in *x* direction has shown approximately 19% higher stiffness, 25% lower strength than soft story due to higher story height and 3% lower stiffness, 25% lower strength than the Ref building. But the most unfavourable case is soft story due to both absence of infill walls and higher height of the ground story. The capacity curve of 6-story SS-H-W building has shown approximately 81% lower strength and 19% lower stiffness than Ref 6 story building, and capacity curve of 3 story SS-H-W building has shown 61.3% lower strength and 62.5% lower stiffness than capacity curve of Ref 3 story building in *y* direction.
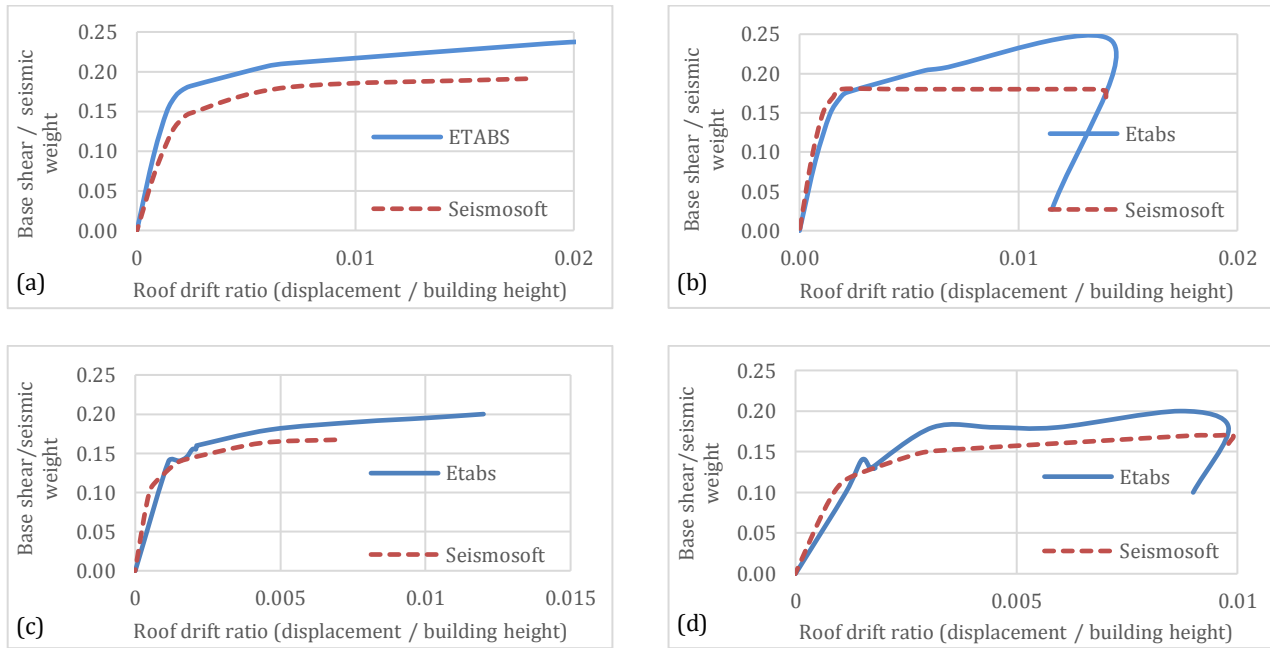
Fig. 10. Comparison between Etabs and Seismosoft analysis results:
(a) Ref 3-story, *x*-direction; (b) Ref 3-story; *y*-direction; (c) Ref 6-story, *x*-direction; (d) Ref 6-story, *y*-direction.
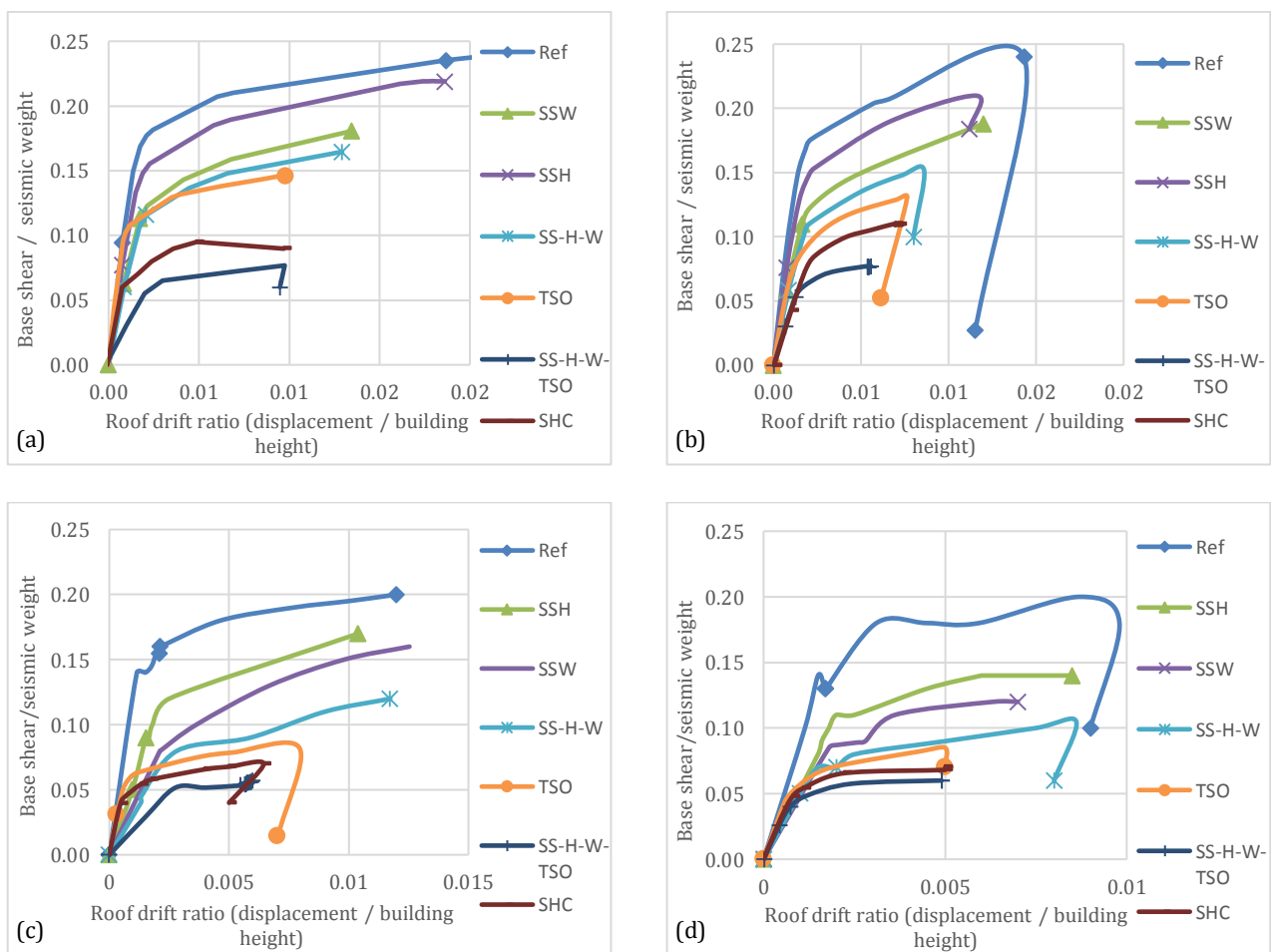

Fig. 11. Capacity curves of: (a) 3-story frames *x*-direction; (b) 3-story frames *y*-direction;
(c) 6-story frames *y*-direction; (d)6- story frames, *y*-direction.

Two sided overhang irregularity is found to be more damaging than soft story irregularity, it lowers more the performance of the building. Capacity curve of the 3 story TSO frame in *x* direction shows 60% lower strength and 100% lower stiffness that the Ref frame in *x* direction. For the 6 story TSO frame it shows 78.5% lower stiffness and 150% lower strength in comparison with Ref 6 story frame in *x* direction.

Soft story with two sided overhang irregularity is found to be more damaging than soft story, short column and two sided overhang irregularities. Capacity curve of the 3 story SS-H-W-TSO in *x* direction shows 182.4% lower strength and 100% lower stiffness than the Ref frame in x direction. The 3 story SS-H-W-TSO in y direction has shown 212.5% lower strength and 116.7% lower stiffness than the Ref frame in Y direction. For the 6 story case it shows 92% lower stiffness, 300% lower strength and 90% lower stiffness and 233% lower strength than 6 story Ref frame, for *x* and *y* direction respectively.

Short column irregularity both softens and weakness the system as shown in the comparison graphs above, Figs. 11(a-d). Capacity curve of the 3 story SHC frame shows 100% lower stiffness, 152.6% lower strength and 62.5% lower stiffness and 127% lower strength than 3 story Ref frame, for x and y direction respectively. Capacity curve of the 6 story SHC frame shows 92.3% lower stiffness, 207% lower strength and 90% lower stiffness and 185% lower strength than 6 story Ref frame, for *x* and *y* directions respectively. From the results it is observed that SS-H-W-TSO and SHC frames are more vulnerable during earthquakes similar to other studies (Inel et al., 2007).

In Table 2 below is shown the summary of the results, stiffness and strength of each one of the considered frames compared to Ref 3 and 6 story frames respectively. From the results it is observed that SS-H-W-TSO and SHC frames are more vulnerable during earthquakes.

Table 2. Comparison of stiffness and strength capacities with Ref frame.

	3-Story frames in x direction	Stiffness in comparison with Ref frame	Strength in comparison with Ref frame
3-Story frames in *x* direction	Ref	=%	=%
	TSO	<100%	<60%
	SSH	<11.1%	<9.1%
	SSW	<53.8%	<29.7%
	SS-H-W	<53.8%	<45.5%
	SS-H-W-TSO	**<100%**	**<182.4%**
	SHC	<100%	<152.6%
3-Story frames in *y* direction	Ref	=%	=%
	TSO	<73.3%	<85.2%
	SSH	<8.3%	<19.0%
	SSW	<8.3%	<31.5%
	SS-H-W	<62.5%	<61.3%
	SS-H-W-TSO	**<116.7%**	**<212.5%**
	SHC	<62.5%	<127.0%
6-Story frames in *x* direction	Ref	=%	=%
	TSO	<78.5%	<150%
	SSH	>11%	<21%
	SSW	>3%	<25%
	SS-H-W	=%	<60%
	SS-H-W-TSO	**<92.3%**	**<300%**
	SHC	<92.3%	<207%
6-Story frames in *y* direction	Ref	=%	=%
	TSO	<90%	<135.3%
	SSH	<11.8%	<35.1%
	SSW	<35.7%	<60%
	SS-H-W	<18.8%	<81%
	SS-H-W-TSO	**<90%**	**<233%**
	SHC	<90%	<185%

3.1. Capacity spectrum method

In order to get the performance point of each of the considered frames, the capacity spectrum method is used. Capacity curve is expressed in terms of spectral displacement and spectral acceleration, positioned in *x*- and *y*- axis, respectively. Then performance point is the intersection of the capacity curve with a modified response spectrum (ATC-40, 1996). Performance point on a capacity curve can also be determined by the ETABS program for a specified elastic spectrum.

In order to get the performance point of the considered frames two response spectrums are used considering two different Codes, Eurocode 8 (2004) and Seismic Albanian Codes (KTP-N2-89, 1989). Parameters of the considered Response spectrum consist of:

Acceleration - 0.25g; soil type – C; behaviour factor (*q*) = 4, spectrum type -1

In Fig. 12 it is seen that for the considered parameters two different response spectrums are generated based on Eurocode 8 (2004) and KTP Codes (KTP-N2-89, 1989). Demand spectrum is based on elastic response which is divided with damping reduction factors C_a and C_v factors which are achieved during constant acceleration and velocity respectively. In order to achieve the reduced response spectrum the below Table 3, is considered in which are given the correspondences between selected response spectrums parameters and reduction factors.
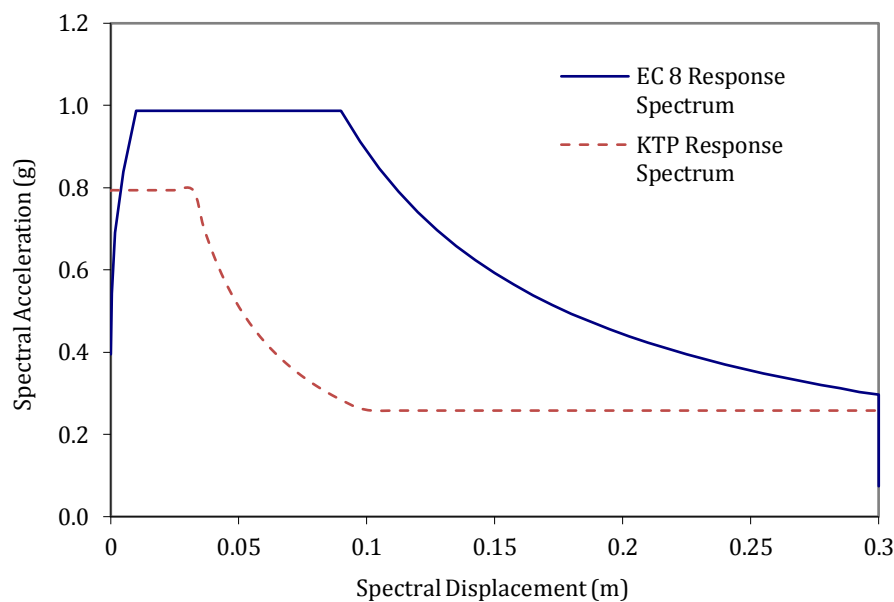
Fig. 12. Considered response spectrums for EC 8 and KTP.

Table 3. Seismic value correspondences (ATC-40, 1996).

Cases	C_a	C_v		A_0	S(T)
a	0.4	0.3		0.40	For soil type 1, T_b=0.3
b	0.4	0.4	Correspond to	0.40	For soil type 2, T_b=0.4
c	0.4	0.6		0.40	For soil type 3, T_b=0.6

*A_0- Seismic zone coefficient

In the study "c" case is considered with reduction factors C_a=0.4 and C_v=0.6 which correspond to soil type 3 and T_b=0.6.

In the below graphs Figs. 13-16 are shown the performance points of the Ref 3 and 6-story frame considering the spectrum from both Codes (EC 8 and KTP), intersection between capacity curve and demand spectrum.

For the 3-story Ref frame in *x* direction, using EC 8, performance point is found at S_a=0.23 and S_d=0.14.

For the 3-story Ref frame in *x* direction, using KTP response spectrum, performance point is found at S_a=0.18 and S_d=0.08.

For the 6-story Ref frame in *x* direction, using EC 8, performance point is found at S_a=0.19 and S_d=0.165. For the 6-story Ref frame in *x* direction, using KTP response spectrum, performance point is found at S_a=0.18 and S_d=0.12.

4. Conclusions

This study assesses the seismic performance of low and mid-rise frames represented by 3- and 6- story frames, respectively. These frames represent the major building stock in Albanian construction industry. Seismic performance of the considered frames is assessed by considering nonlinear behaviour of reinforced concrete components and masonry infill walls.
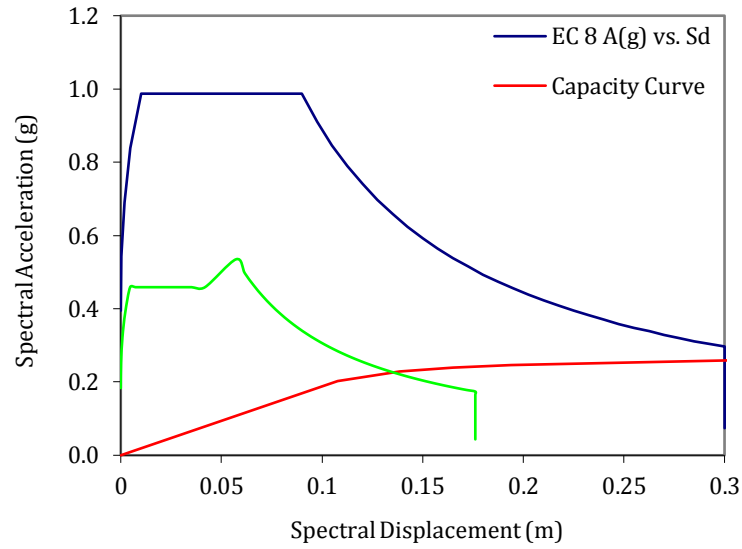
Fig. 13. Performance point of Ref 3 story *x*-direction frame EC 8.
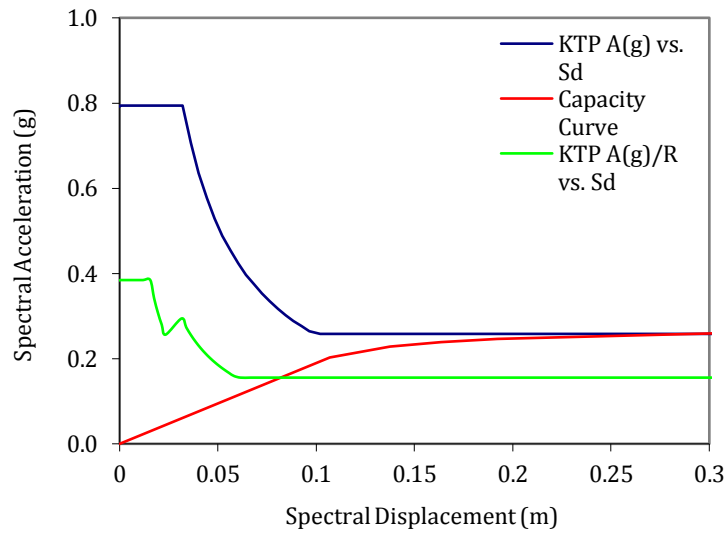
Fig. 14. Performance point of Ref 3 story *x*-direction frame KTP.
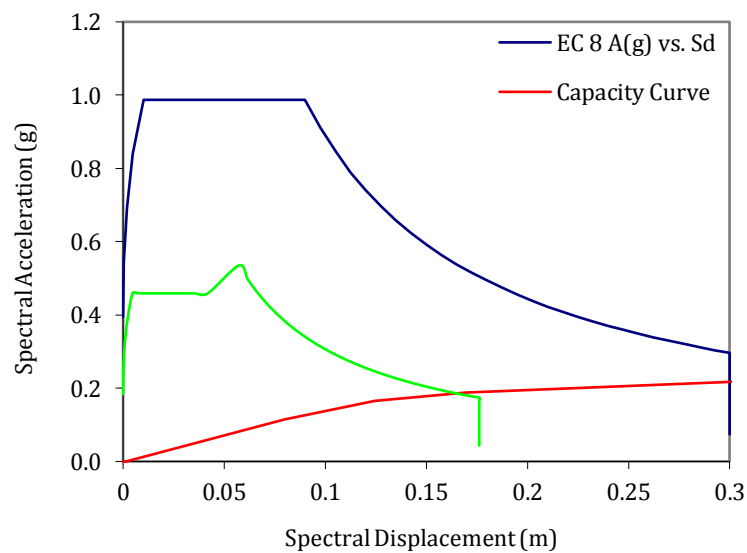
Fig. 15. Performance point of Ref 6 story *x*-direction frame EC 8.
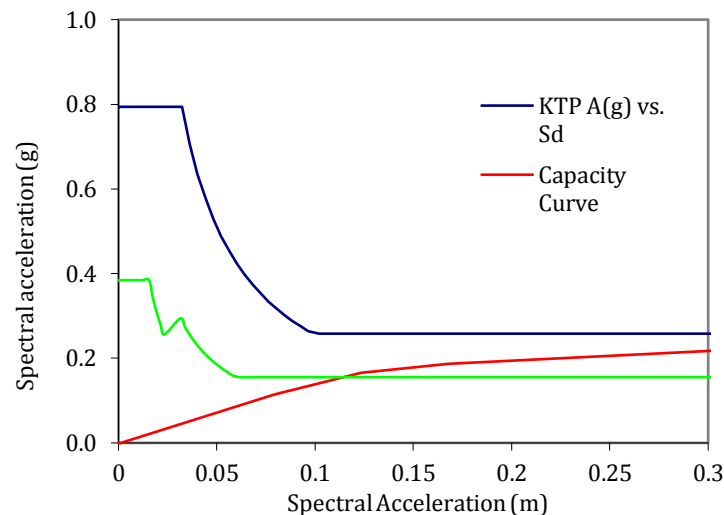
Fig. 16. Performance point of Ref 6 story *x*-direction frame KTP.

In this study masonry infill walls were modelled as diagonal strut elements in accordance with FEMA-356 (2000) guidelines. Regular and irregular frames are considered. Irregular frames are obtained as a result of different structural irregularities, implemented to the regular frames. Structural irregularities taken in consideration for this study are: soft story, heavy overhangs, short column. Effect of structural irregularities and performance of the considered frames are achieved by using capacity curves of the frames and performance point by considering two different response spectrums, from Eurocode 8 (2004) and KTP codes (KTP-N2-89, 1989). Calibration of results is checked by using two different programs ETABS and Seismosoft to analyse the reference frames, 3 and 6 story. The observations and findings of the current study are briefly summarized in the following:

Presence of structural irregularities in reinforced concrete buildings decreases the performance of the frame by lowering its lateral load bearing and displacement capacity. Structural irregularities have almost the same effect in both low and mid-rise frames represented by 3- and 6- story frames.

Soft story with two sided overhangs and short column are the most detrimental irregularities for both low and mid-rise buildings.

Soft story due to lack of masonry infill walls at the ground story is found to be more damaging than soft story because of higher ground story height.

From the achieved performance points it was observed that demands of Eurocode 8 are higher than KTP codes, representing higher values for both spectral acceleration and spectral displacement.

REFERENCES

Altuntop MA (2007). Analysis of building structures with soft stories. *M.Sc. thesis,* Atılım University, Turkey.

Apostolska R, Necevska-Cvetanovska G, Cvetanovska J, Gjorgjievska E (2010). Influence of Masonry Infill on Seismic Performance of RC Frame Buildings. Skopje: Institute of Earthquake Engineering and Engineering Seismology (IZIIS), "Ss.Cyril and Methodius" University, Skopje, Republic of Macedonia.

ATC-40 (1996). Seismic Evaluation and Retrofit of Concrete Buildings. Applied Technology Council, Redwood City, CA.

Bachmann H (2002). Seismic Conceptual Design of Buildings – Basic Principles for engineers, architects, building owners, and authorities'. Federal Department of Foreign Affairs (DFA), Zurich.

Dolsek M, Fajfar P (2000). Soft story effects in uniformly infilled reinforced concrete frames. *Journal of Earthquake Engineering*, 5(1), 1-12.

Eurocode 8 (2004). Design of structures for earthquake resistance - Part 1: General rules, seismic actions and rules for buildings. European Committee for Standardization, Brussels.

FEMA-356 (2000). Prestandart and commentary for seismic rehabilitation of buildings. Federal Emergency Management Agency, Washington (DC).

Inel M, Bilgin H, Ozmen HB (2007). Orta yükseklikteki betonarme binaların deprem performanslarının afet yönetmeliğine göre tayini. *Pamukkale Universitesi Muhendislik Bilimleri Dergisi*, 13(1), 81-89.

Inel M, Ozmen HB (2008). Effect of infill walls on soft story behavior on mid-rise RC buildings. *Proceedings of the 14th World Conference on Earthquake Engineering*, Beijing, China, Paper No. 05-01, p. 279.

KTP-N2-89 (1989). Albanian Seismic Code: Earthquake Resistant Design Regulations. Seismic Center, Academy of Science of Albania. Department of Design, Ministry of Construction, Tirana, Albania

Sattar S, Liel AB (2010). Seismic performance of reinforced concrete frame structures with and without masonry infill walls. *9th U.S. National and 10th Canadian Conference on Earthquake Engineering*, Toronto, Canada.

Semnani SJ, Rodgers JE, Burton HV (2014). Conceptual Seismic Design Guidance for New Reinforced Concrete Framed Infill Buildings. GeoHazards International, CA.

Sonmez E (2013). Effect of infill wall stiffness on the behavior of reinforced concrete frames under earthquake demands. *M.Sc. thesis,* Graduate School of Engineering and Sciences of İzmir Institute of Technology, İzmir.

Tena-Colunga A (2004). Evaluation of the seismic response of slender, setback RC moment-resisting frame buildings designed according to the seismic guidelines of a modern building code. *13th World Conference on Earthquake Engineering*, Vancouver, B.C., Canada.

Uruci R, Bilgin H (2016). Effects of soft storey irregularity on RC building response. *3rd International Balkans Conference on Challenges of Civil Engineering*, Epoka University, Tirana, Albania, 136-143.

Vahidi EK, Malekabadi MM (2009). Conceptual investigation of short-columns and masonry infill frames effect in the earthquakes. *International Journal of Civil and Environmental Engineering,* 3(11), 472-477.

Varadharajan S (2014). Study of Irregular RC Buildings under Seismic Effect. *Ph.D thesis*, National Institute of Technology Kurukshetra, Kurukshetra.

Research Article

Performance based study on the seismic safety of buildings

Zinnur Çelik [a,*], Ahmet Budak [b]

[a] *Department of Civil Engineering, Pasinler Vocational School, Atatürk University, 25300 Erzurum, Turkey*
[b] *Department of Civil Engineering, Atatürk University, 25240 Erzurum, Turkey*

A B S T R A C T

In the scope of this study, information has been provided on the Static Pushover Analysis which is a nonlinear deformation controlled analysis method and the Capacity Spectrum Method used to determine the performance point. In this study, static pushover analysis was made on a six-storey building with reinforcement concrete frame system by changing the materials, steel rebars and soil characteristics. The building's capacity curves were drawn and decided according to different concrete and reinforcement groups. Furthermore the performance points of different classes of concrete were studied according to three seismic effect levels. In the case of a decrease in the reinforcement strength, a decrease of approximately 30% occurs in the base shear force. If the concrete strength is increased, an increase of 11% occurred in the base shear force. Consequently, in the comparisons made with five different concrete groups and two different reinforcement groups, rather than the increase in the strength of the concrete, an increase in the reinforcement strength was observed to be more effective on the structural capacity. Furthermore, local soil classifications were observed to be the most significant point regarding peak displacement.

1. Introduction

The concept of performance is a newly developed concept in earthquake engineering and was developed in the first place to determine the safety of the existing buildings. However, the possibility to use this method in new buildings came into question. It is estimated that in addition to classic rules, dimensioning principles based on the concept of performance that require a more detailed examination shall be included in the future earthquake regulations. Performance based design can be seen as an expansion of the classic design concept (Celep and Kumbasar, 2004).

It has been known for a long time that the constructional damage which occurs during earthquakes is not directly related with the fact that structural elements' current strength capacity has been exceeded under the equivalent seismic loads described by the regulations, but with the fact that the deformation capacity of structural elements which are expected to display ductile behaviour has been exceeded (ATC, 1996; FEMA, 1997-2000).

The global pushover curve obtained as a result of the pushover analysis indicates the nonlinear change of the base shear strength according to the horizontal displacement at the topmost storey. However the main purpose of the Nonlinear Static Method consists of determining the seismic demand concerning maximum displacements and especially concerning maximum plastic displacements under the effect of a given seismic effect, then to compare these demand values with deformation capacities defined for selected performance levels defined for selected performance levels and thus to evaluate its structural performance. Looking from this perspective, the pushover curve does not have a significance beyond showing the nonlinear strength and displacement capacities of the load-bearing system. As a consequence the coordinates of the pushover curve are transformed into modal displacement corresponding to the displacement of the normalized strength of the same system equivalent single degree of freedom system represented by the system's first natural vibration mode and modal pseudo-acceleration coordinates corresponding

to the normalized strength of the same system. Subsequently, using nonlinear spectral displacement which represents the largest displacement in the equivalent single degree of freedom system under the earthquake effect, the seismic demands indicated above are obtained. Different methods are used to define nonlinear spectral displacement in Displacement Coefficient Method and Capacity Spectrum Method developed as two different versions of the nonlinear static method (Aydınoğlu, 2003).

In this analysis where the nonlinear behaviour at critical sections is modelled with plastic hinge model, the amplitude of the horizontal loads that affect the system is increased step by step according to a distribution that does not change during the analysis or according to distributions that vary at each step and internal strengths, displacements and plastic deformations are calculated at each step.

The Nonlinear Static Method which is briefly summarized above no doubt represents a very important development which can be described as a revolution in earthquake engineering practice and earthquake engineers encouraged by successful applications made on simple systems want to use this method in a more widespread manner. However an important matter which should be stated at this point is the fact that many problems and restrictions concerning Nonlinear Static Method based on static pushover analysis have not been overcome (Krawinkler and Seneviratna, 1998). In fact, the theoretical foundations of the method have not been entirely revealed yet and the development of the model continues to remain intuitive to a great extent (Elnashai, 2002).

2. Static Pushover Analysis

In their studies, to show the effect of torsion irregularity which causes large damages on building systems during an earthquake on the level of damage (Moghadam and Tso, 1995) have emphasized the use of nonlinear analysis methods in no symmetrical structures.

In their study (Kilar and Fajfar, 1997) have presented a simple method for the nonlinear static pushover analysis of no symmetrical structures exposed to uniformly increasing horizontal loads (static pushover analysis). They have said that this method was designed as part of new methods for the valuation of buildings and their seismic designs. They have stated that the structure consists of planar macro elements. In the study, for each planar macro element, a bilinear or multilinear displacement of base shear strength – peak point was assumed. By performing a step-by-step analysis they have calculated the estimated relation between the base shear strength and peak point displacement. In order to reduce certain restrictions of the nonlinear static pushover analysis methods they have developed a new nonlinear static pushover analysis. The methods they have developed, at various levels of the ultra-elastic behaviour of the building, depending on the various rigidities of the elements and the characteristics of the building system, takes into account the variance of the horizontal load distribution and includes higher mode effects.

In order to investigate the conformity of the 3-dimensioned nonlinear static pushover analyses in the seismic analysis of asymmetric structures, the results obtained from nonlinear dynamic analyses were analysed up to the maximum peak displacement and were compared with static incremental pushover analysis results (Faella and Kilar, 1998). In their study (Kalkan and Kunnath, 2007) states the necessity to estimate correctly the seismic demand parameters of critical and basic components in performance based design methods. It was mentioned that nonlinear static procedures were widely used in engineering practices in estimating seismic demands of buildings.

Irtem and Hasgul (2009), in their studies, have aimed to evaluate and compare the structural reaction requests obtained from the capacity spectrum method (CSM) proposed in ATC-40 which is one of the nonlinear static analysis procedures (NSPs) and from displacement coefficients methods (DCM) proposed in FEMA 356. For this purpose, they have studied three dimensionally three multiple storied reinforcement concrete buildings of different characteristics. In order to determine the nonlinear behaviour of buildings under lateral strengths, they obtained base shear strength-peak displacement relations (capacity curves) by a static pushover analysis containing P-delta curves. By taking to account four different seismic risk levels, they determined building performances by using CSM and by using DCM results determined through previous studies. By taking to account multiple-storied reinforcement concrete buildings and comparing structural reaction amounts (such as plastic rotations, storey displacement) they have studied the impacts of different NSP's in the performance evaluation of the buildings.

2.1. Capacity spectrum method

Two methods can be implemented for the existing reinforcement concrete buildings, linear and nonlinear analysis. In the linear analysis method, only the material's behaviour within linear limits is taken into account. As the nonlinear behaviour of the material is not taken to account additional capacity cannot be used in the elements. The linear analysis includes processes that use static horizontal strength, dynamic horizontal strength and demand-capacity ratios. There are several methods in the nonlinear analysis. These methods are, in the general sense, based on "Time History" analysis. However, as this analysis method is competed method which cannot be widely used, simplified nonlinear analysis methods are used. In the "Capacity Spectrum Method" which is one of the simplified linear analysis methods, in order to find the maximum displacement the intersection point between the capacity (pushover) curve and the reduced demand spectrum curve is found and nonlinear analysis is performed (Kesim, 2005).

The Capacity Spectrum Method is based on the principle that the maximum displacements which may occur in the building due to a certain seismic movement and the building's horizontal load bearing capacity are interconnected. Inelastic deformations occur on a building which is subject to increased seismic loads and these

deformations increase the damping of the building which in turn decreases the building's displacement demand with the increased damping. Capacity Spectrum method consists of finding especially the performance point that is the point where the capacity spectrum (produced from the capacity curve) and the elastically reduced demand spectrum (corrected by taking to account the nonlinear behaviour) (Özdaş, 2006).

The first phase of the nonlinear incremental pushover analysis is to obtain the building's capacity curve. In order to obtain the capacity curve of the building, the building is observed until it reaches the limit situation under the fixed vertical loads and horizontal equivalent seismic loads (F) increasing from the ground by calculating according to the incremental pushover analysis where the effect of geometrical changes on the equation of equilibrium are taken to account. As a result of these changes, it is the capacity curve obtained by uniting geometrically the intersection points ($\delta_ç$) of the total base shear strengths (Vt) which are reaction strengths for each load value in the vertical direction and the roof (peak)

displacements in the horizontal directions. This curve is called the pushover curve (Özdaş, 2006).

By using the exiting relation between the base shear strength (Vt) which impacts a building a building and the top floor i.e. the roof displacement ($\delta_ç$) it is transformed to a spectrum curve at the spectral acceleration (Sa) and spectral displacement (Sd) plane.

In order to determine the seismic effect, a seismic demand spectrum with 5% damping is created by using the C_A and C_V seismic coefficients. C_A represents the effective maximum acceleration coefficient, C_V, the spectrum value of the 5% damped system which has a period of 1 sec. The seismic coefficients of C_A and C_V are determined according to the seismic region where the building is located, to its distance to a known seismic source, the type of earthquake which is to be used in the calculations and the soil classification. The N_A and N_V coefficients which represent the distance to the earthquake source are found in the Table 1, according to the building's distance to the earthquake source and the type of earthquake which shall be created by the source.

Table 1. Near source factors (ATC–40, 1996).

Seismic source type	Closest distance to known seismic source							
	≤ 2 km		5 km		10 km		≥ 15 km	
	N_A	N_V	N_A	N_V	N_A	N_V	N_A	N_V
A: Faults that are capable of producing large magnitute events	1.50	2.00	1.20	1.60	1.00	1.20	1.00	1.00
B: All faults other than types A and C	1.30	1.60	1.00	1.20	1.00	1.00	1.00	1.00
C: Faults that are not capable of producing large magnitute events	1.00	1.00	1.00	1.00	1.00	1.00	1.00	1.00

In order to compare S_a and the traditional demand spectrum given in period format with the capacity spectrum which is in the spectral acceleration – spectral displacement format it has to be transformed to the ADRS format. The period and spectral acceleration which is on any point on the traditional demand spectrum is turned into spectral acceleration-spectral displacement.

If the horizontal coordinates of the intersection between the capacity spectrum and the reduced demand spectrum is not different than the spectral displacement value with an interval of ±5% the performance point which is found can be accepted as the real performance point. If the horizontal coordinates of the intersection between the capacity spectrum and the reduced demand spectrum is not within the above indicated interval, a new point is determined and the iteration is continued. The performance point is defined as the maximum value of displacement which may occur in the building in the face of the ground motion.

3. Pushover Analysis Details

The 6-storey reinforcement concrete building with frame system examined in the study has been dimensioned adequately regarding geometry and materials to ensure ductility requirements. The building's concrete group is between C14–C30, the concrete steel rebar group was selected as S420. The characteristics of the reinforcement concrete six-storey building with frame system are shown in Table 2. The section of the reinforcement concrete six-storey building with frame system are shown Fig. 1. Static pushover analyses are performed in the SAP2000 V14 program.

In the study, static pushover analyses of a 6-storey reinforcement concrete building with frame system were made according to 5 different concrete classes. In this study, plastic hinge hypothesis has been used to take into account the nonlinear behaviour. According to that, it is assumed that the plastic deformations are assumed to occur at regions named as plastic hinge and acted with

linear elasticity at other sections. In order to determine the seismic performance of buildings, the limit rotation values belonging to different performance levels were used for columns and beams indicated in ATC 40.

Table 2. Characteristics of six-storey reinforcement concrete structure.

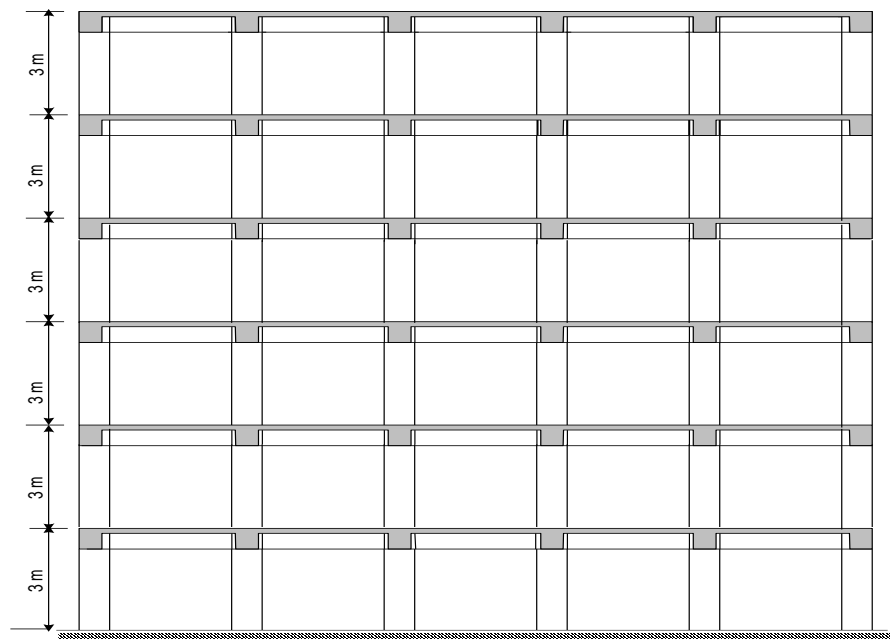|	
Earthquake zone	2
Effective ground acceleration coefficient	0.30
Earthquake zone coefficient	0.30
Soil group	Z2
Building importance coefficient	1
Earthquake type	Design earthquake
Spectrum characteristic periods	T_A: 0.15 T_B: 0.40
Conveyor system behavior coefficient	8
Concrete group	C14, C16, C20, C25, C30
Steel rebar group	S420 – S220

Fig. 1. Section of six-storey reinforcement concrete structure.

As a result of the static pushover analysis the base shear strength in the case of the building's failure and the peak displacement were found. In the analysis made for the C30 concrete class, the relation between the base shear strength and displacement is shown in Fig. 2. The failure load of the building is 14,443 kN. The peak displacement corresponding to this failure load is 0.304 m. As a result of the static pushover analysis 333 plastic hinges at immediate use performance level (B–IO), 361 of them at the controllable damage interval (IO–LS), 47 of them at limited safety interval (LS–CP) have occurred and the building has reached the state of failure.

In the analyses made for the concrete groups of C25, C20, C16 and C14, the relation between base shear strength and displacement were shown in the Figs. 3, 4, 5 and 6.

Static pushover analysis was made above for five different concrete classes and the results that are obtained are shown in Fig. 7. When the results of the capacity curves are evaluated, depending on the increase of concrete quality, an increase occurs in the base shear strength compensate by the building.

Base shear strength and displacements according to the different concrete and S420 reinforcement classes are shown in Table 3. When the table is observed, it is seen a decrease of 8.46% is observed in the base shear strength when the concrete class is reduced from C30 to C14. Whereas in the peak displacements a decrease of 11.84% occurs.
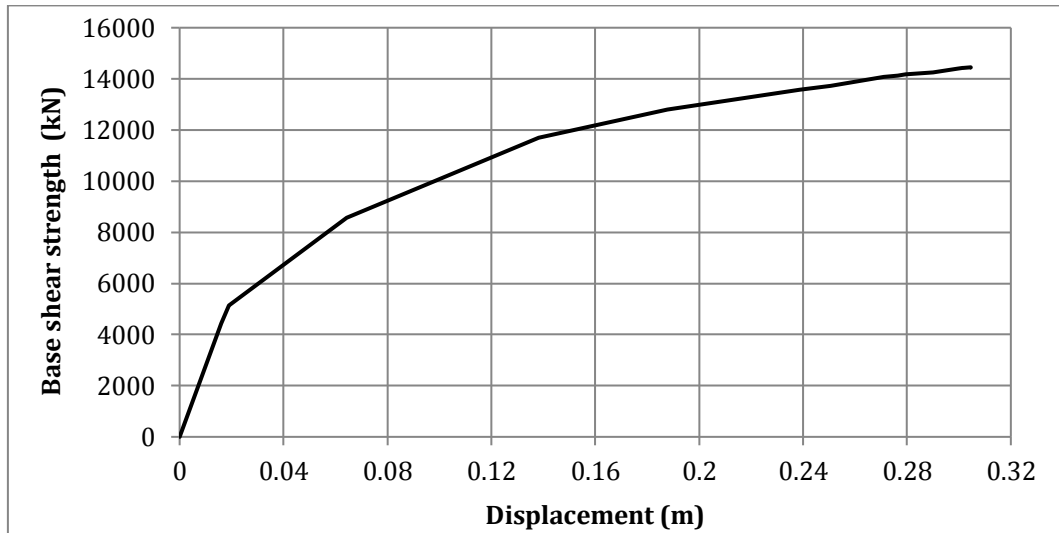
Fig. 2. Capacity curve for C30 concrete group.
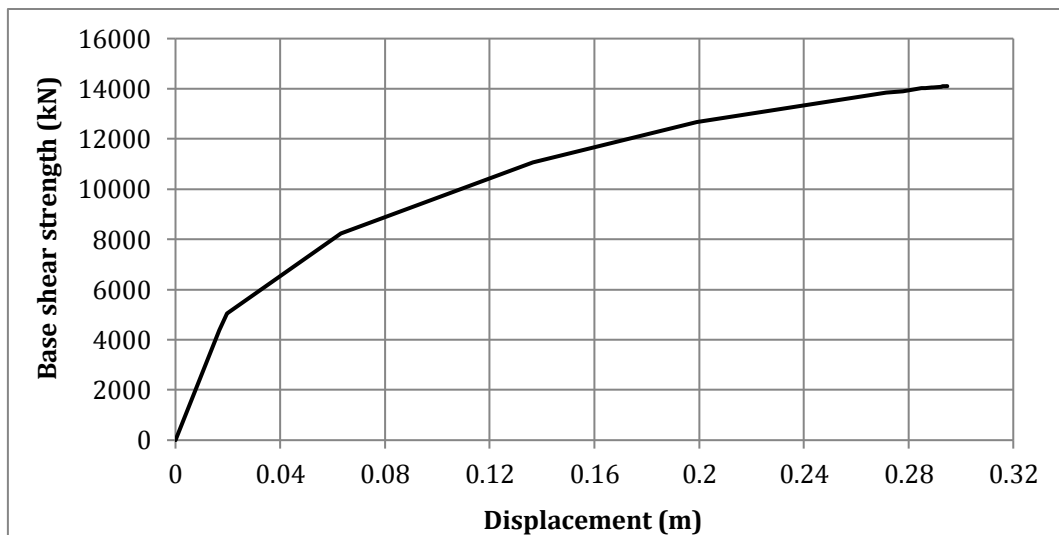
Fig. 3. Capacity curve for C25 concrete group.
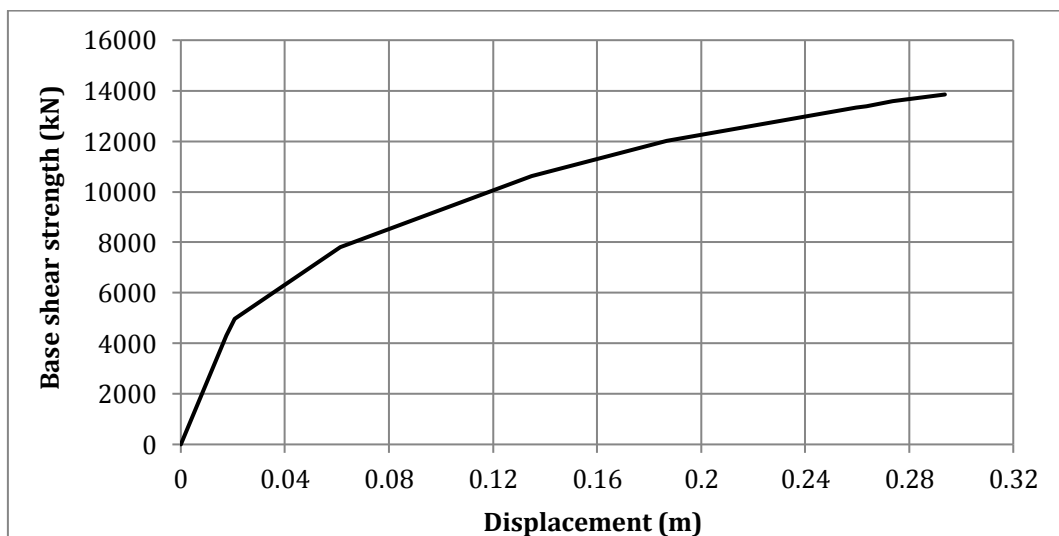
Fig. 4. Capacity curve for C20 concrete group.
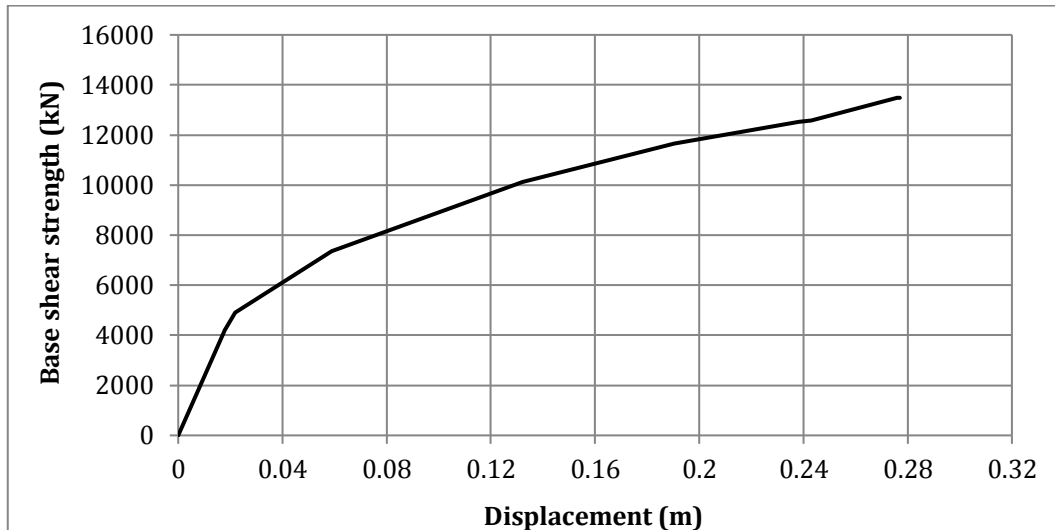
Fig. 5. Capacity curve for C16 concrete group.
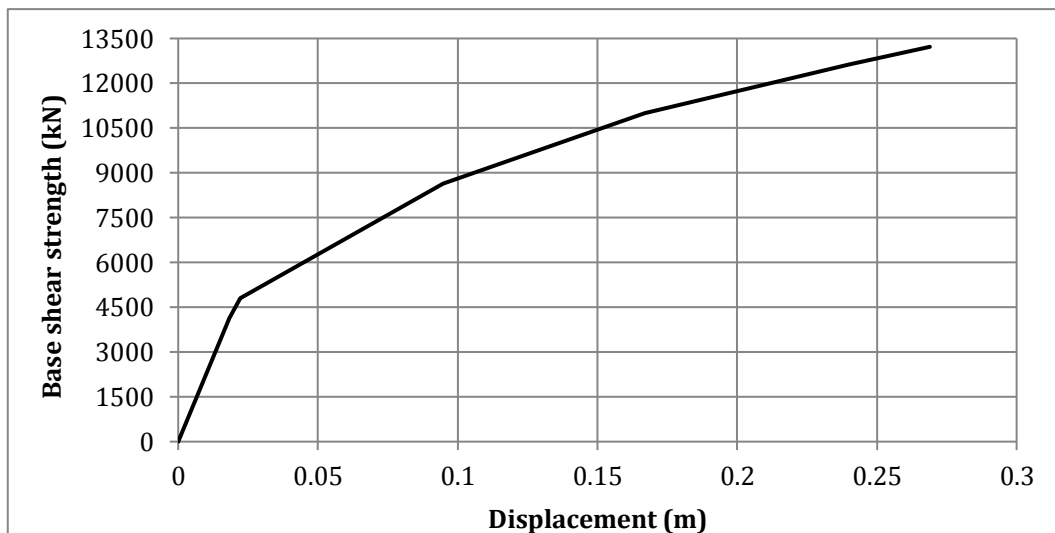
Fig. 6. Capacity curve for C14 concrete group.
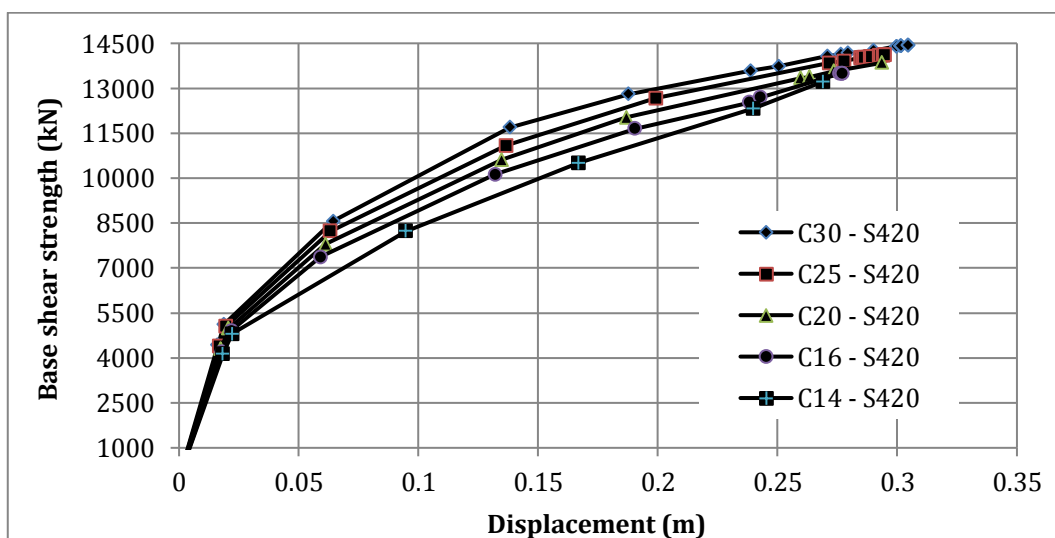
Fig. 7. Capacity curve for concrete group (S420).

Table 3. Base shear strength and displacement according to the concrete and reinforcement classes.

Concrete and steel rebar group	V (kN)	D (m)	Reduction ratios of base shear strength according to C30 concrete group (%)	Reduction ratios of peak displacements relative to C30 concrete group (%)
C30–S420	14,443	0.304	-	-
C25–S420	14,108	0.297	2.32	3.29
C20–S420	13,850	0.291	4.11	4.28
C16–S420	13,486	0.276	6.63	9.21
C14–S420	13,220	0.268	8.46	11.84

An increase in the concrete quality, by increasing the number of plastic hinges ensures that it carries heavier loads. This situation is shown in the Table 4.

The reinforcement group is taken as S220, the capacity curves obtained for different concrete classes have also been shown on a single graph Fig. 8. When the figure is studied, an increase in the base shear strength is observed depending on the increased concrete quality.

Base shear strength and displacements according to the different concrete and S220 reinforcement classes are shown in Table 5. When the table is observed, it is seen a decrease of 12.58% is observed in the base shear strength when the concrete class is reduced from C30 to C14. Whereas in the peak displacements a decrease of 19.56% occurs. As a result, base shear strength and displacements according to the different concrete and S220-S420 reinforcement classes are shown in Fig. 9.

Table 4. Distribution of plastic sections according to the concrete and reinforcement classes.

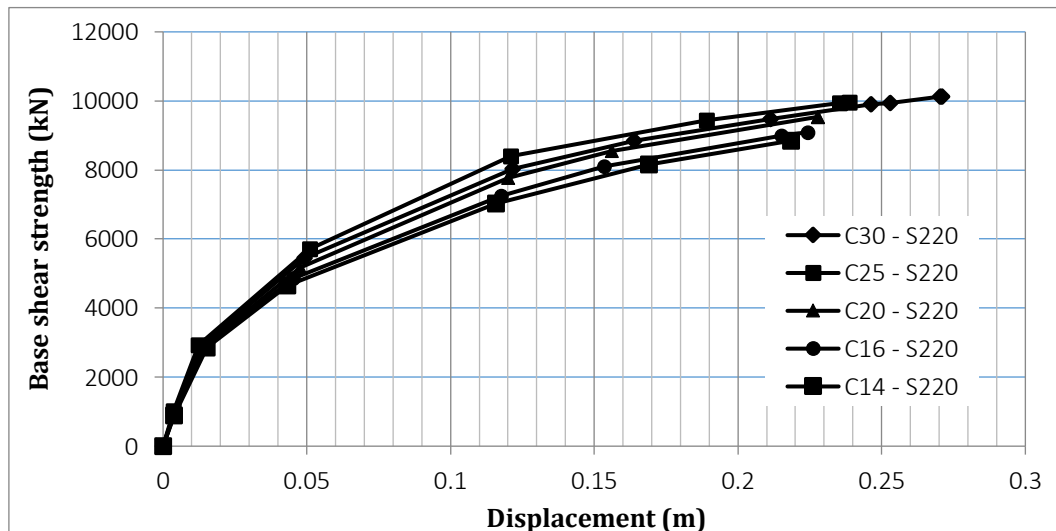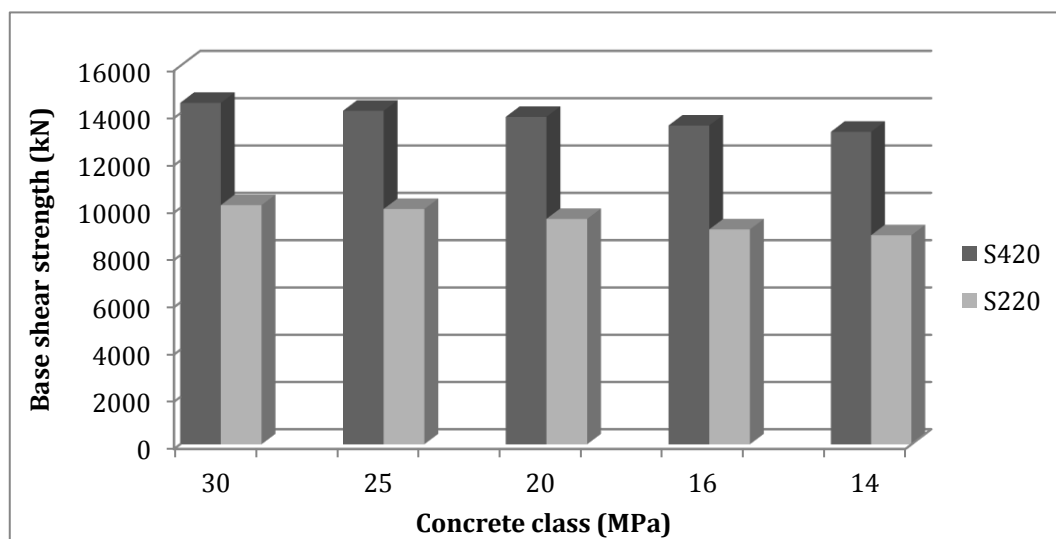| Concrete group	B - IO	IO - LS	LS - CP
C30	333	361	47
C25	325	385	22
C20	320	393	19
C16	310	409	13
C14	298	428	7

Fig. 8. Capacity curve for concrete group (S220).

Table 5. Base shear strength and displacement according to the concrete and reinforcement classes.

Concrete and steel rebar group	V (kN)	D (m)	Reduction ratios of base shear strength according to C30 concrete group (%)	Reduction ratios of peak displacements relative to C30 concrete group (%)
C30–S220	10,122	0.271	-	-
C25–S220	9,957	0.238	1.63	12.18
C20–S220	9,538	0.227	5.77	16.24
C16–S220	9,095	0.224	10.15	17,.34
C14–S220	8,849	0.218	12.58	19.56

Fig. 9. Base shear strength and displacements according to the different concrete and S220-420 reinforcement classes.

4. Conclusions

In the study, the six-storey building with concrete frame system has been designed to provide high ductility requirements. The results obtained in the scope of this study are indicated below.

When the results of the capacity curves are evaluated, depending on the increase of concrete quality, an increase occurs in the base shear strength compensate by the building. In the event of using concrete class C30 instead of C14, an increase of 8.46% occurred in the base shear strength. There is an increase of 11.84% in peak displacement.

According to the result obtained in this study, while 7 plastic hinges occur at the limited safety interval (LS – CP) for concrete class C14, this value becomes 47 for the concrete class C30. The increase in the quality of concrete results in an increase in the number of plastic hinges causing it to carry more loads.

As a result of the analyses which have been made, in the event of the reinforcement strength being S220 instead of S420, the base shear strength compensate by the C30 concrete class has decreased by 30%.

When the capacity curves are evaluated, depending on the increase in the concrete quality it is seen that the building requires more horizontal loads for the same displacement value. When the demand base shear strengths at the performance point of the building which examined in the study in the event of considering a concrete class of C30 instead of C14 the base shear strength was observed to increase by 8% in utilization earthquake, by 11% in design earthquake, by 14% in the maximum earthquake. For all studied concrete classes performance levels are in Immediate Use state.

REFERENCES

ATC 40 (1996). Seismic evaluation and retrofit of concrete buildings. Applied Technology Council, Redwood City, California, USA.

Aydınoğlu MN (2003). Yapıların deprem performansının değerlendirilmesi için artımsal spektrum analizi yöntemi. *Beşinci Ulusal Deprem Mühendisliği Konferansı*, İstanbul, Turkey. (in Turkish)

Celep Z, Kumbasar N (2004). Deprem Muhendisliğine Giris ve Depreme Dayanıklı Yapı Tasarımı. Beta Yayınevi, İstanbul, Turkey. (in Turkish)

Elnashai AS (2002). Do we really need inelastic dynamic analysis? *Journal of Earthquake Engineering*, (6), 123-130.

Faella G, Kilar V (1998). Asymmetric multi-storey R/C frame structures: push- over versus nonlinear dynamic analysis. *Proceedings of the Eleventh European Conference on Earthquake Engineering*, Paris, France.

FEMA 273 (1997). NEHRP Guidelines for the Seismic Rehabilitation of Buildings. Federal Emergency Management Agency, Washington D.C., USA.

FEMA 356 (2000). Prestandard and Commentary for the Seismic Rehabilitation of Buildings. Federal Emergency Management Agency, Washington D.C., USA.

Irtem E, Hasgul U (2009). Investigation of effects of nonlinear static analysis procedures to performance evaluation on low-rise RC buildings. *Journal of Performance of Constructed Facilities*, 23(6), 456-466.

Kalkan E, Kunnath SK (2007). Assessment of current nonlinear static procedures for seismic evaluation of buildings. *Engineering Structures*, 29(3), 305-316.

Kesim B (2005). Statik İtme Analizi ile Mevcut bir Betonarme Binanın İncelenmesi. *M.Sc. thesis*, İstanbul Technical University, İstanbul, Turkey. (in Turkish)

Kilar V, Fajfar P (1997). Simple push-over analysis of asymmetric buildings. *Earthquake Engineering and Structural Dynamics*, 26(2), 233-249.

Krawinkler H, Seneviratna GDPK (1998). Pros and cons of a pushover analysis of seismic performance evaluation. *Engineering Structures*, 20(4-6), 452-464.

Moghadam AS, Tso WK (1995). 3-D pushover analysis for eccentric buildings. *Proceedings of 7th Canadian Conference on earthquake engineering*, Montreal, Canada.

Özdaş A (2006). Asmolen Döşemeli Betonarme Yapıların Doğrusal Olmayan Statik İtme Analizi. *M.Sc. thesis*, Karadeniz Technical University, Trabzon, Turkey. (in Turkish)

Research Article

Use of geosynthetics to reduce the required right-of-way for roadways and railways

Niyazi Özgür Bezgin *

Department of Civil Engineering, İstanbul University, 34320 İstanbul, Turkey

A B S T R A C T

Roadway and railway routes require a right-of-way (ROW) to provide the necessary width for the required travelled way, drainage and earthwork. Correct understanding of ROW along a route is necessary in order to establish a correct width for the intended transportation corridor. Availability of land becomes scarce and cost of land increases in urban zones. Therefore, the costs of establishing a ROW in rural areas and in urban areas are not the same. Earthworks are an important component of route establishment. The required excavations and fills necessitate the use of proper side slopes for the stability of the excavation or the fill. These side slopes directly relate to the mechanical properties of the soil and the depth of the earthwork. This study provides a quantitative and a qualitative understanding of the ROW requirements of roadways and railways and the influence of the earthworks on the determined values of the ROW. The study further investigates the benefits of using geogrids to reduce the necessary ROW for a transportation route through finite element analysis.

1. Introduction

Establishment of roadway and railway routes necessitates the establishment of the required ROW for the placement of the requirements of a particular transportation corridor. Transportation engineers respond to the estimated transportation demand along a route by providing a capacity that produces a satisfactory level-of-service (LOS). A common representation of the transportation capacity is the number of units that can be transported per unit value time. The number of roadway lanes and railroad tracks of a route, along with the values of curvatures and profile slopes influence the capacity of a route.

The width required for the establishment of roadways and railways must be correctly estimated to facilitate sufficient space for the requirement of the route. On the other hand, the scarcity of land in urban grounds increase the construction costs per distance as opposed to route construction costs in rural grounds. Therefore, one must correctly estimate the required ROW and investigate means to reduce the required ROW in order to establish

an economic and an achievable transportation route. The following section offers simple parametric tools to estimate the required ROW for roadways and railways. The discussion included in the section that follows provides an analytical insight into how geogrid reinforcements can effectively reduce the required ROW.

2. Right-of-way Requirements for Railways and Roadways

Roadways and railways have unique requirements for their cross-sections. The following two subsections discuss these requirements and the necessary widths for their establishment.

2.1. Roadways

Roadways are built to provide a link between locations where there is a mutual traffic demand. Number of lanes and the geometric alignment requirements are

based on the design LOS and the estimated volume of traffic. A roadway section includes the travelled way which is provided by the total number of lanes, shoulder lanes that provide refuge for disabled vehicles and emergency vehicles and a median that includes space for barriers, drainage and future space for possible lane additions. The lane widths typically vary from 3.3 m or 3.5 m to 3.75 m and the shoulder widths vary up to 3 m. The median width is variable depending on the route conditions, the costs of providing the ROW and the projected traffic conditions. Fig. 1 shows a typical cross section for a 4-lane and 2-way roadway. The left part of the figure represents the roadway on a fill and the right side of the figure represents the roadway within a cut.
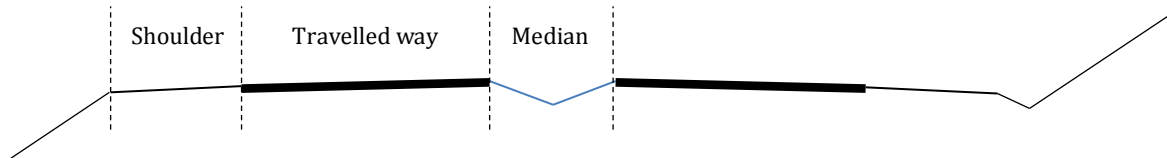

Fig. 1. Typical components of two-way and 4-lane roadway (TEM, 2002).

One needs to account for all the aspects of roadway construction in order to have an understanding of the required ROW to satisfy all the needs of the roadway. The geography along which the route is placed may require extensive earthwork to attain the design gradients. To this end, cuts and fills may take place along the route that requires an extended ROW for the route. The following list summarizes the necessary components of a roadway and Eq. (1) provides an equation to estimate the required ROW.

A. Lane width.
B. Shoulder lane width.
C. Number of lanes.
D. Number of shoulder lanes. 1 or 2.
E. Median width.
F. Total drainage width of the drainage channels.
G. Depth of the cut.
H. Depth of the fill.
İ. Side slope of the cut: vertical depth/lateral extent.

J. Side slope of the fill: vertical height/lateral extent.
K. Number of cut slope. 0, 1 or 2.
L. Number of fill slope. 0, 1 or 2.

Eq. (1), proposed by the author presents the required width of the ROW for a roadway. This is a general equation that can be modified to reflect the particular earthwork conditions. For instance, if the earthwork is completely on a fill then $L=2$ and $K=0$. If half of the earthwork is on a fill and half of it is on a cut then $L=1$ and $K=1$. If the earthwork is completely within a cut then $L=0$ and $K=2$.

$$\text{ROW} = A \times C + B \times D + E + F + (G/I) \times K + (H/J) \times L . \qquad (1)$$

Table 1 is a summary of ROW requirements for a 4-lane and two-way roadway with the given properties with varying depths of cut and fills. The roadway cross sections presented in Table 1 is composed of either a total fill or a total cut. The requirements are determined based on the proposed Eq. (1).

Table 1. ROW requirements for a roadway.

Lane width (m)	Shoulder width (m)	Median width (m)	Number of lanes	Number of shoulders	Total width of drainage ditch (m)	Width of super-structure (m)	
3.6	2	1	2	2	2	14.2	

Depth of cut (m)	Depth of fill (m)	Slope of cut	Slope of fill	Total width of the cut (m)	Width of the fill (m)	Width of ROW in only cut (m)	Width of ROW on only fill (m)
2	2			4	8	18.2	22.2
4	4	1	1/2	8	16	22.2	30.2
6	6			12	24	26.2	38.2
2	2			8	12	22.2	26.2
4	4	1/2	1/3	16	24	30.2	38.2
6	6			24	36	38.2	50.2

The required side slopes for cuts and fills is partly a question of geotechnical engineering and partly a question of traffic safety engineering. The cuts and fills must take place under correct slope angles to provide long term stability and safety of the slope. On the other hand, the slopes must be forgiving to vehicles that have gone astray and prevent them from over turning down a fill slope and crashing into a cut slope. The required side slope for a cut in a particular geotechnical material is typically higher than the required side slope of a fill consisted of the same

materials, since the angle of repose of the undisturbed material within the cut is typically higher than the angle of repose of the disturbed material that is excavated and compacted for the fill. With this understanding, Table 1 provides an insight into the variation of the need for a ROW for a roadway of a certain superstructure width. Table 1 indicates that the earthwork requirements are an important component of the required ROW of a roadway.

2.2. Railways

Trains provide transport of goods and people between locations along a guided way. Railways are a common form of guided ways that are mainly composed of ballasted superstructures. But contemporary guided ways are increasingly using slab tracks and more recently the electrified tracks that are a part of magnetic levitation superstructures. Experimental studies for an alternative land transport named the "Hyperloop" that rely on magnetic levitation within a vacuumed tube as a guide way is underway.

Design of the railway superstructure takes into account the expected wheel forces, the design speeds and the design traffic. A ballasted railway superstructure consists of the rails, the ties supporting the rails, the ballast surrounding and underneath the ties and the sub-ballast layers. The number of tracks thus attained determines the superstructure width of the railway. Along with the drainage and earthwork slope requirements, the required ROW of railways is typically lower than roadways, which is beneficial from an environmental and civil engineering point of view. Nevertheless, the ROW required for a railway route is much greater than what is typically needed for the individual railway tracks.

Fig. 2 is a sketch of the components of a ballasted track. A ballasted railway superstructure consists of the sub-ballast layer, underlying a ballast layer within which the sleepers that support the rails are embedded. The sub-ballast provides frost protection, drainage and filtering to the ballast layer and together with the ballast layer they distribute the bearing stresses underneath the sleepers to acceptable levels on the sub-grade. The sub-grade may be a fill or natural ground in a cut. The width of a normal gauge track as measured from the centerlines of the rails is 1.5 m.
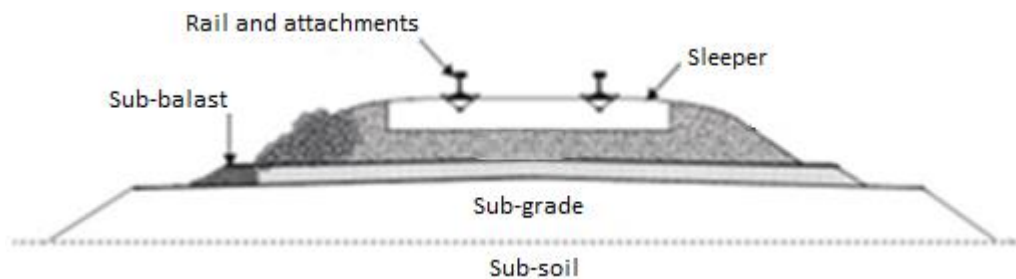

Fig. 2. Components of a ballasted railway track.

The following list provides the details of the components and their design values that determine the required ROW of a particular section along a railway route.
1. Sleeper width: 240 cm – 280 cm
2. Shoulder ballast width: Up to 50 cm.
3. Ballast depth: 30 cm minimum.
4. Sub-ballast depth: Variable. 20 cm minimum.
5. Sub-ballast slope: 1:2 typical.
6. Ballast side slope: 1:2 typical.
7. Safety walkway width: Variable. 1 m minimum preferred.
8. Number of tracks: Variable. Contemporary railways minimum 2 tracks.
9. Minimum centerline distance between tracks: Variable.
10. Drainage channel width: Variable
11. Depth of cut: Variable.
12. Depth of fill: Variable
13. Side slope of the cut: Variable.
14. Side slope of the fill: Variable.

The variables listed above are simplified for design and based on the simplification; the variables below become effective on the ROW requirement.
A. Minimum distance between the centerline of the track and the edge of the superstructure.
B. Minimum distance between the centerlines of the tracks.
C. Number of tracks.
D. Required total width of drainage channels.
E. Depth of the cut.
F. Depth of the fill.
G. Side slope of the cut: vertical depth/lateral extent.
H. Side slope of the fill: vertical height/lateral extent.
I. Number of cut slope. 0, 1 or 2.
J. Number of fill slope. 0, 1 or 2.

Eq. (2), proposed by the author, presents the required width of the ROW for a railway. Similar to Eq. (1), this is a general equation that can be modified to reflect the particular earthwork conditions. For instance, if the earthwork is completely on a fill then I=0 and J=2. If half of the earthwork is on a fill and half of it is on a cut then I=1 and J=1. If the earthwork is completely within a cut then I=2 and J=0.

$$ROW = A \times 2 + B \times (C\text{-}1) + D + (E/G) \times I + (F/H) \times J. \qquad (2)$$

Fig. 3 is a sketch of a two-track ballasted railway showing the centerline spacing of the two tracks and the edge distances of a track centerline with respect to the boundary of the track superstructure. The variations in the specified dimensions occur according to the design train speeds for the tracks, with higher dimensions affiliated with higher speeds.
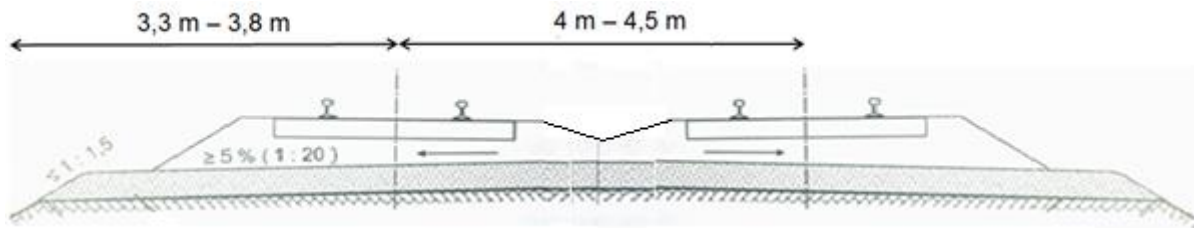
Fig. 3. Two track ballasted railway superstructure (Lichtberger, 2011).

Fig. 4 is a photograph showing the ROW required for a cut. Notice that the required width is directly proportional to the cut depth and the needed ROW is much greater than the width required for only the railway superstructure. Table 2 presents the ROW requirements for a double track high speed railway route for varying cut and fill values.

Fig. 4. Perspective of a double track railway route through a cut (UDH, 2012).

Table 2. ROW requirements for a railway.

	Track centerline distance (m)	Track edge distance (m)	Number of tracks	Total width of drainage ditch (m)	Width of super-structure (m)	
	4.5	3.8	2	2	12.1	
Depth of cut (m)	Depth of fill (m)	Slope of cut	Slope of fill	Total width of the cut (m)	Width of the fill (m)	Width of ROW in only cut (m)	Width of ROW on only fill (m)
2	2			4	8	16.1	20.1
4	4	1	1/2	8	16	20.1	28.1
6	6			12	24	24.1	36.1
2	2			8	12	20.1	24.1
4	4	1/2	1/3	16	24	28.1	36.1
6	6			24	36	36.1	48.1

3. Expropriation Costs for Transportation Routes

Previous discussions highlight the need and the necessity of sufficient ROW for roadways and railways. The required ROW becomes especially critical in urban grounds where the land costs are much higher compared to rural areas. Urban land values can be up to 20 times more than rural land values (McCarthy, 2001). Recent studies indicate ROW acquisition costs up to 20% of the total projects costs in urban areas (Balcı, 2010).

One must remember that although the transportation routes appear as curvilinear lines on a map, they do have a width. The fact that their widths are very low compared to the length of a route sometimes result in under-

estimating the needs for width that becomes problematic especially in urban grounds where the cost of land and the cost of acquisition is high. 1-m extra ROW width per kilometer of route amounts to an extra 1,000 m² land per km of route.

The following section provides a simple analytic explanation for the benefits of reinforcing the earth to reduce the required ROW, which has useful implications in the establishment of transportation routes.

4. Effects of Geogrids in Earthworks

Uses and benefits of geogrids in transportation applications is plenty. From a mechanical point of view, the interlocking and interaction between a geogrid layer embedded in soil with the surrounding soil domain is essential to the improvement of the soil resistance. Deformations within a soil domain under applied loads generate tensile stresses within the embedded geogrid layer interacting with the soil. The tension in the geogrid provides confinement on the soil. This confinement changes the positioning of the failure planes and delays their development via increasing the shear strength of the soil. Typical application of geogrids involve parallel placement at 30 cm–60 cm intervals up to a 70% height of the strengthened and stiffened soil mass (EBGEO, 2011).

A thorough numeric investigation of the stress states within a soil mass requires a sophisticated analysis program than can conduct a non-linear, discrete element contact stress variation analysis. In the absence of such a program, a simple linear continuous domain analysis yielded a limited but effective understanding of the influence of the side slopes of a fill on its stability and the benefits of geogrids in achieving slope stability.

Finite element models for a 1-m thick and 6-m high sand fill with a unit mass of 2,000 kg/m³ established for a 14-m wide roadway superstructure with variable side slopes provided some understanding of stress distribution within the supported soil mass. The modulus of elasticity of the soil is taken as E=204 MPa. The unit of the stresses presented in the finite element analysis results is kg-f/m² (kilogram-force per m²). The internal friction angle of the modeled soil is 30°. In order to shorten the run time of the models, only half of the soil mass is modeled. In other words, the left edges of the models are the centerlines of the modeled superstructure.

Fig. 5 shows the results obtained for the case of the absence of a side slope. In this case where the soil mass is vertical, it is a known fact that the soil mass fails and reaches stability at its natural angle of repose. Fig. 5(c) reveals the upper portion of the stress field that tends to "flow over" the bottom part of the soil. The maximum top displacement is 2 mm and the highest vertical stress developed at the bottom is 12,000 kg-f/m². The highest lateral shear stress at the bottom right corner of Fig. 5(c) is 2,040 kg-f/m².
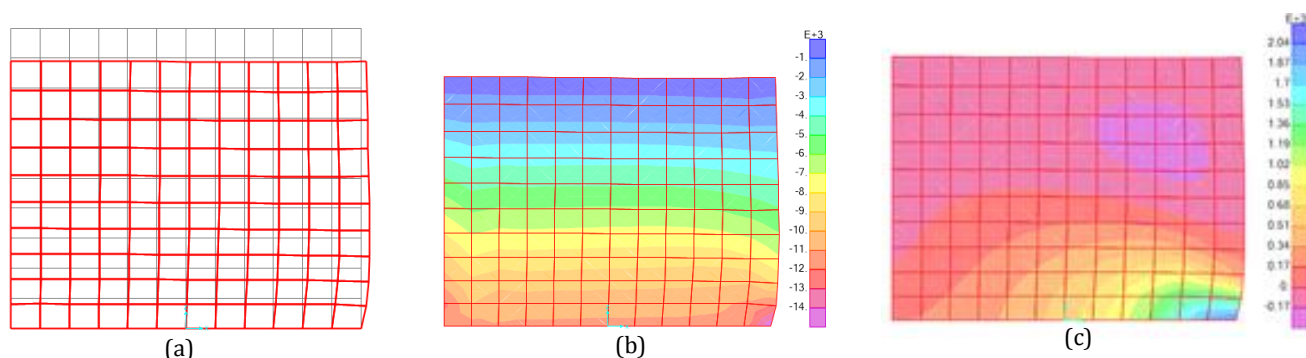

(a)   (b)   (c)

Fig. 5. FEM analysis results of a half model: (a) Deformed shape of a 14 m wide superstructure on a 6 m fill; (b) Vertical normal stress distribution; (c) Shear stress distribution.

Figs. 6 and 7 shows the FE analysis results of a similar soil mass, where the side slopes of the fill is lowered to 1:1 (vertical : lateral) with a slope angle of 45°. If one compares Fig. 7 with Fig. 5(c), the part of the soil mass that moves rightwards is resisted by the abutting soil at the toe of the slope. The provided support for the tendency to flow to the right is shown by the dashed arrow emanating from the toe region of the side slope. The maximum shear stress at the toe of the slope develops within the slope that is slightly to the left of the slope boundary and reduces to 1,300 kg-f/m² for the case of 1:1 slope. In other words, the side slope provides some form of an abutment to the lateral shearing deformation and provides confinement to the lateral spread of the vertical height of the fill.

Fig. 8 shows the FE model for the case where the side slope is further lowered to 1:2 with a slope angle of 26.5°.

Fig. 10 yields that the shear stresses at the toe are lower than the values shown at Fig. 7 for the case with a side slope of 1 to 1. The vertical displacement is about 1.5 mm. The maximum shear stresses at the toe of the slope further reduces to 960 kg-f/m² for the case of 1:2 slope and the region of maximum shear stress is further pushed inwards the fill thereby highlighting the effect of decreased side slopes on the developing shears and improved slope stability.

The stress distribution within the soil mass can be changed by introducing the horizontal stiffening action of geogrids. Fig. 11 shows a soil mass with a 1:1 slope stiffened by layers of geogrids placed at 60 cm intervals along the depth of the soil mass. The stiffness of the geogrids are 1,000 kg-f/mm per meter geogrid width. Compared to Fig. 7, the geogrids provides a second source of lateral confinement to the fill additionally to

the abutment effect of the side slope. The center of lateral tensile forces on the geogrids distribute the maximumum areas of the shear stresses to approximately mid-height of the fill and the interior of the toe of the fill. The confinement due to geogrids

represented by the dotted arrow is added to the abutting support provided by the toe of the fill. Compared to the shear stresses presented in Fig. 7, the use of geogrids have reduced the shear stresses approximately 23%.
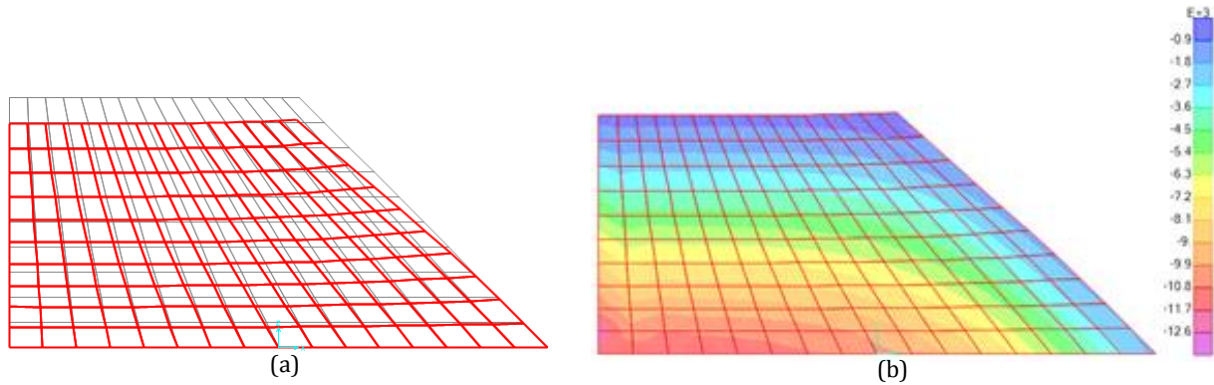
Fig. 6. FE model analysis results of a half model with a 1:1 side slope:
(a) Deformed shape of a 14 m wide superstructure on a 6 m fill; (b) Vertical normal stress distribution.
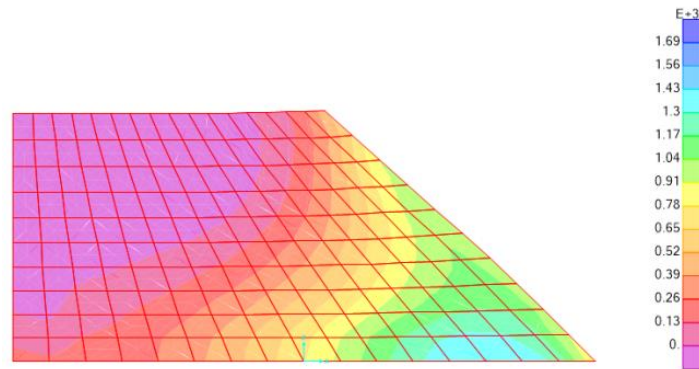

Fig. 7. FEM analysis result of a half model with a 1:1 side slope for shear stress distribution.
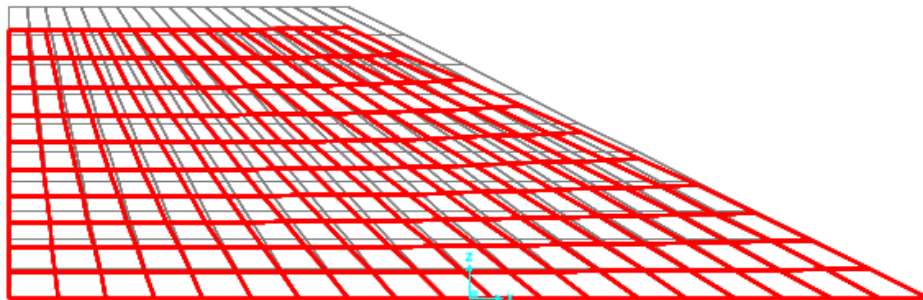

Fig. 8. FE model deformation results of a half model with 1:2 side slope.
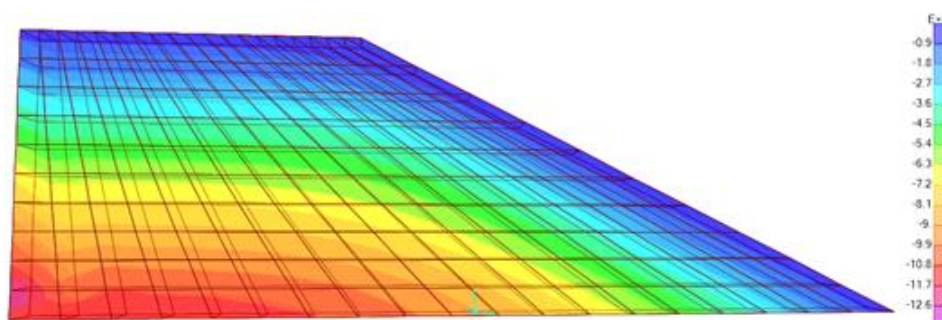

Fig. 9. FE model analysis results of vertical stress distribution of a half model.
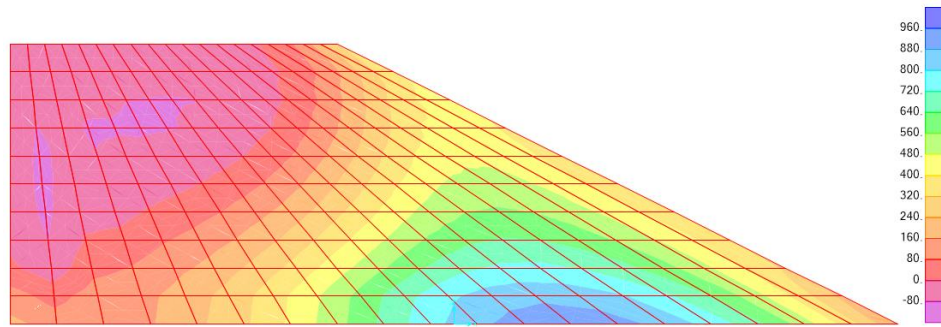
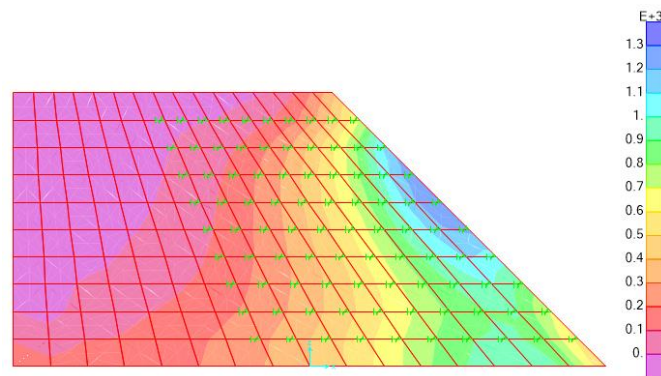**Fig. 10.** FE model analysis results of shear stress distribution of a half model.

Fig. 11. FE model analysis results of shear stress distribution of a geogrid supported soil mass.

5. Conclusions

This paper qualitatively discussed the issue or ROW for roadways and railways. For the investigated cases, the ROW needs were shown to be able to reach up to 350% of the size of the transportation superstructure depending on the depth of the earthwork. The costs of land and expropriation in urban settings, which could be up to 20 times more than values in rural environments, require means and methods to limit the required ROW for a particular route. Simple qualitative and quantitative finite element analysis showed how the geogrids could change the stress distribution in soil masses thereby providing alternative earthwork designs which require lower ROW values. Inclusion of geogrids provides a lateral confinement to the soil masses thereby increasing the internal shear strength of the supported soil mass. Inclusion of the geogrids reduced and distributed the shear stresses within the soil mass such that a 1:1 slope became possible with respect to a 1:2 slope for a 6-m high fill, resulting in a total reduction of 12-m for the required ROW for a 14 m wide railway superstructure.

REFERENCES

Balcı E (2010). Kamulaştırma Maliyetinin İstanbul Ulaşım Yatırımlarına Etkilerinin İncelenmesi. *M.Sc. Thesis*, Bahçeşehir University, İstanbul.

Bernhard L (2011). Track Compendium. Eurail Press.

EBGEO (2011). Recommendations for Design and Analysis of Earth Structures using Geosynthetic Reinforcements. Ernst and Sohn.

McCarthy P (2001). Transportation Economics Theory and Practice: A Case Study Approach. Blackwell.

Trans-European North-South Motorway (TEM) (2002). Standards and Recommended Practice and Recommended Practice, Third Edition.

Ulaştırma, Denizcilik ve Haberleşme Bakanlığı (2012). Türkiye'de Demiryolları ve Politikaları.

Research Article

Eigenvector and eigenvalue analysis of thick plates resting on elastic foundation with first order finite element

Yaprak I. Özdemir *

Department of Civil Engineering, Karadeniz Technical University, 61080 Trabzon, Turkey

ABSTRACT

The purpose of this paper is to study free vibration analysis of thick plates resting on Winkler foundation using Mindlin's theory with first order finite element, to determine the effects of the thickness/span ratio, the aspect ratio, subgrade reaction modulus and the boundary conditions on the frequency parameters of thick plates subjected to free vibration. In the analysis, finite element method is used for spatial integration. Finite element formulation of the equations of the thick plate theory is derived by using first order displacement shape functions. A computer program using finite element method is coded in C++ to analyze the plates free, clamped or simply supported along all four edges. In the analysis, 4-noded finite element is used. Graphs are presented that should help engineers in the design of thick plates subjected to earthquake excitations. It is concluded that 4-noded finite element can be effectively used in the free vibration analysis of thick plates. It is also concluded that, in general, the changes in the thickness/span ratio are more effective on the maximum responses considered in this study than the changes in the aspect ratio.

ARTICLE INFO

1. Introduction

Plates are structural elements which are commonly used in the building industry. A plate is considered to be a thin plate if the ratio of the plate thickness to the smaller span length is less than 1/20; it is considered to be a thick plate if this ratio is larger than 1/20 (Ugural, 1981).

The dynamic behavior of thin plates has been investigated by many researchers (Warburton, 1954; Leissa, 1973, 1977a, 1977b, 1981a, 1981b, 1987a, 1987b; Caldersmith, 1984; Sakata and Hosokawa, 1988; Providakis and Beskos, 1989a, 1989b; Ayvaz and Durmuş, 1995; Lok and Cheng, 2001; Grice and Pinnington, 2002; Si et al., 2005). There are also many references on the behavior of the thick plates subjected to different loads. The studies made on the behavior of the thick plates are based on the Reissner-Mindlin plate theory (Reissner, 1945, 1947, 1950; Mindlin, 1951). This theory requires only C^0 continuity for the finite elements in the analysis of thin and thick plates. Therefore, it appears as an alternative to the

thin plate theory which also requires C^1 continuity. This requirement in the thin plate theory is solved easily if Mindlin's theory is used in the analysis of thin plates. Despite the simple formulation of this theory, discretization of the plate by means of the finite element comes out to be an important parameter. In many cases, numerical solution can have lack of convergence, which is known as "shear-locking". Shear locking can be avoided by increasing the mesh size, i.e. using finer mesh, but if the thickness/span ratio is "too small", convergence may not be achieved even if the finer mesh is used for the low order displacement shape functions.

In order to avoid shear locking problem, the different methods and techniques, such as reduced and selective reduced integration, the substitute shear strain method, etc., are used by several researchers (Hinton and Huang, 1986; Zienkiewich et al., 1971; Bergan and Wang, 1984; Ozkul and Ture, 2004; Hughes et al., 1977). The same problem can also be prevented by using higher order displacement shape function (Özdemir et al., 2007). Wanji and Cheung (Wanji and Cheung, 2000) proposed a new

quadrilateral thin/thick plate element based on the Mindlin-Reissner theory. Soh et al. (2001) improved a new element ARS-Q12 which is a simple quadrilateral 12 DOF plate bending element based on Reissner-Mindlin theory for analysis of thick and thin plates. Brezzi and Marini (2003) developed a locking free nonconforming element for the Reissner-Mindlin plate using discontinuous Galarkin techniques. Belounar and Guenfound (2005) improved a new rectangular finite element based on the strain approach and the Reissner-Mindlin theory is presented for the analysis of plates in bending either thick or thin. Vibration analysis made by Raju and Hinton (1980), they presented natural frequencies and modes of rhombic Mindlin plates. Si et al. (2005) studied vibration analysis of rectangular plates with one or more guided edges via bicubic B-spline method, Cen et al. (2006) developed a new high performance quadrilateral element for analysis of thick and thin plates. This distinguishing character of the new element is that all formulations are expressed in the quadrilateral area co-ordinate system. Shen et al. (2001) studied free and forced vibration of Reissner-Mindlin plates with free edges resting on elastic foundations. Woo et al. (2003) found accurate natural frequencies and mode shapes of skew plates with and without cutouts by p-version finite element method using integrals of Legendre polynomial for p=1-14. Qian et al. (2003) studied free and forced vibrations of thick rectangular plates using higher-order shear and normal deformable plate theory and meshless Petrov-Galarkin method. Özdemir and Ayvaz (2009) studied shear locking free earthquake analysis of thick and thin plates using Mindlin's theory. GuangPeng et al. (2012) studied free vibration analysis of plates on Winkler elastic foundation by boundary element method. Fallah et al. (2013) analyzed free vibration of moderately thick rectangular FG plates on elastic foundation with various combinations of simply supported and clamed boundary conditions. Governing equations of motion were obtained based on the Mindlin plate theory. Jahromi et al. (2013) analyzed free vibration analysis of Mindlin plates partially resting on Pasternak foundation. The governing equations which consist of a system of partial differential equations are obtained based on the first-order shear deformation theory. Özgan and Daloğlu (2013) studied

free vibration analysis of thick plates on elastic foundations using modified Vlasov model with higher order finite elements, also same authors (2015) studied the effects of various parameters such as the aspect ratio, subgrade reaction modulus and thickness/span ratio on the frequency parameters of thick plates resting on Winkler elastic foundations.

The purpose of this paper is to study free vibration analysis of thick plates resting on Winkler foundation using Mindlin's theory with first order finite element, to determine the effects of the thickness/span ratio, the aspect ratio, subgrade reaction modulus and the boundary conditions on the frequency parameters of thick plates subjected to free vibration. A computer program using finite element method is coded in C++ to analyse the plates free, clamped or simply supported along all four edges. In the program, the finite element method is used for spatial integration. Finite element formulation of the equations of the thick plate theory is derived by using first order displacement shape functions. In the analysis, 4-noded finite element is used to construct the stiffness and mass matrices (Özdemir et al., 2007).

2. Mathematical Model

The governing equation for a flexural plate (Fig. 1) subjected to free vibration without damping can be given as;

$$[M]\{\ddot{w}\}+[K]\{w\}=0 \ , \tag{1}$$

where [K] and [M] are the stiffness matrix and the mass matrix of the plate, respectively, w and $\ddot{w}$ are the lateral displacement and the second derivative of the lateral displacement of the plate with respect to time, respectively.

The total strain energy of plate-soil-structure system (see Fig. 1) can be written as;

$$\Pi=\Pi_p+\Pi_s+ V, \tag{2}$$

where Π_p is the strain energy in the plate,

$$\Pi_p = \frac{1}{2}\int_A\left(-\frac{\partial\varphi_x}{\partial x} \quad \frac{\partial\varphi_y}{\partial y} \quad -\frac{\partial\varphi_x}{\partial y}+\frac{\partial\varphi_y}{\partial x}\right)^T E_\kappa\left(-\frac{\partial\varphi_x}{\partial x} \quad \frac{\partial\varphi_y}{\partial y} \quad -\frac{\partial\varphi_x}{\partial y}+\frac{\partial\varphi_y}{\partial x}\right)d_A$$

$$+ \frac{k}{2}\int_A\left(-\varphi_x+\frac{\partial w}{\partial x} \quad \varphi_y+\frac{\partial w}{\partial y}\right)^T E_\gamma\left(-\varphi_x+\frac{\partial w}{\partial x} \quad \varphi_y+\frac{\partial w}{\partial y}\right)d_A \ , \tag{3}$$

where Π_s is the strain energy stored in the soil,

$$\Pi_s =\frac{1}{2}\int_0^H\int_{-\infty}^\infty\int_{-\infty}^\infty \sigma_{ij}\varepsilon_{ij} \ , \tag{4}$$

and V is the potential energy of the external loading;

$$V=-\int_A \bar{q}w d_A \ . \tag{5}$$

In this equation, E_κ and E_γ are the elasticity matrix and these matrices are given below at Eq. (17), $\bar{q}$ shows applied distributed load.
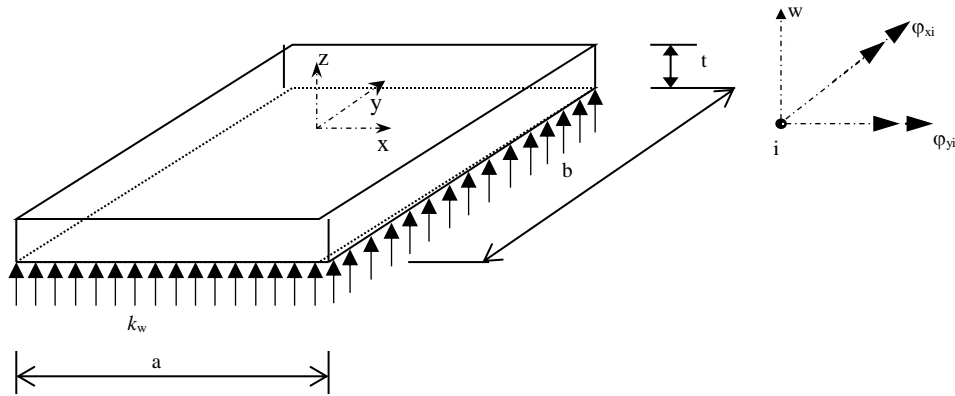
Fig. 1. The sample plate used in this study.

2.1. Evaluation of the stiffness matrix

The total strain energy of the plate-soil system according to Eq. (2) is;

$$U_e = \frac{1}{2}\int_A \left(-\frac{\partial \varphi_x}{\partial x} \quad \frac{\partial \varphi_y}{\partial y} \quad -\frac{\partial \varphi_x}{\partial y}+\frac{\partial \varphi_y}{\partial x}\right)^T E_\kappa \left(-\frac{\partial \varphi_x}{\partial x} \quad \frac{\partial \varphi_y}{\partial y} \quad -\frac{\partial \varphi_x}{\partial y}+\frac{\partial \varphi_y}{\partial x}\right)d_A$$

$$+ \frac{k}{2}\int_A \left(-\varphi_x+\frac{\partial w}{\partial x} \quad \varphi_y+\frac{\partial w}{\partial y}\right)^T E_\gamma \left(-\varphi_x+\frac{\partial w}{\partial x} \quad \varphi_y+\frac{\partial w}{\partial y}\right)d_A + \frac{1}{2}\int_A \left(w_{x,y}\right)^T \mathrm{K}\left(w_{x,y}\right)d_A . \tag{6}$$

At this equation the first and second part gives the conventional element stiffness matrix of the plate, $[k_p^e]$, differentiation of the third integral with respect to the nodal parameters yields a matrix, $[k_w^e]$, which accounts for the axial strain effect in the soil. Thus the total energy of the plate-soil system can be written as;

$$U_e = \frac{1}{2}\{w_e\}^T \left([k_p^e]+[k_w^e]\right)\{w_e\}d_A , \tag{7}$$

where

$$\{w_e\}=[w_1 \quad \varphi_{x1} \quad \varphi_{y1} \quad ... \quad w_n \quad \varphi_{xn} \quad \varphi_{yn}]^T . \tag{8}$$

Assuming that in the plate of Fig. 1 u and v are proportional to z and that w is the independent of z (Mindlin, 1951), one can write the plate displacement at an arbitrary x, y, z in terms of the two slopes and a displacement as follows;

$$\{w, u, v\}=\{w, z\varphi_x, -z\varphi_y\}=\{w, z\frac{\partial \varphi_i}{\partial x}, -z\frac{\partial \varphi_i}{\partial y}\} , \tag{9}$$

where w_0 is average displacement of the plate and, φ_x and φ_y are the bending slopes in the x and y directions, respectively.

The nodal displacements for 4-noded quadrilateral serendipity element (MT4) (Fig. 2) can be written as follows;

$$w=\sum h_{i1}w_i , \quad u=z\varphi_x=z\sum_1^4 h_{i2}\varphi_{xi} ,$$

$$v=-z\varphi_y=-z\sum_1^4 h_{i3}\varphi_{yi} , \quad (i=1, 2, 3, 4) . \tag{10}$$

Nodal actions corresponding to the displacements in Eq. (10) are;

$$\mathrm{pi}=\{p_{i1}, p_{i2}, p_{i3}\}=\{p_{zi}, M_{xi}, M_{yi}\} \quad (i=1, 2, 3, 4) . \tag{11}$$

The symbols p_{zi} denotes a force in the z direction, but M_{xi} and M_{yi} are moments in the x and y directions. Note that these fictitious moments at the nodes are not the same as the distributed moments in the vector M of generalized stresses (Weaver and Johnston, 1984).

The displacement function chosen for this element is;

$$w=c_1+c_2 r + c_3 s + c_4 rs , \tag{12}$$

which is a complete linear of four terms. From this assumption, it is possible to derive the displacement shape function to be;

$$h_i=[h_1, h_2, h_3, h_4] , \tag{13}$$

where

$$h_1 = (0.25) \times (1+r) \times (1+s) ,$$
$$h_2 = (0.25) \times (1-r) \times (1+s) ,$$
$$h_3 = (0.25) \times (1-r) \times (1-s) ,$$
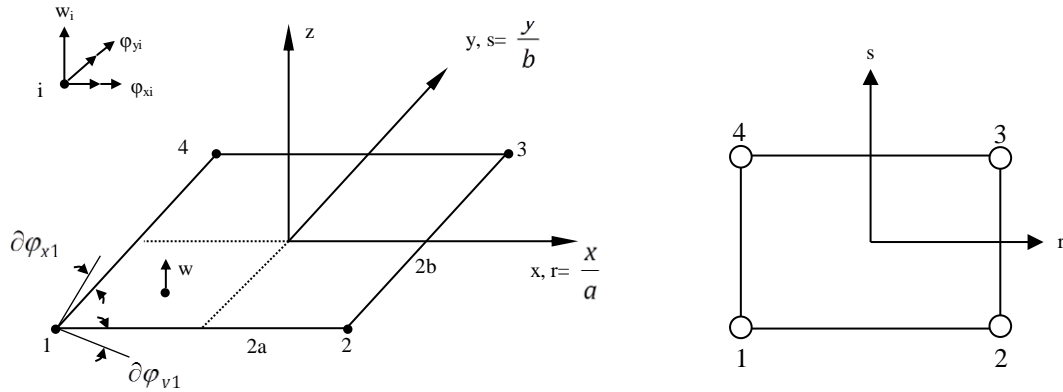$$h_4 = (0.25) \times (1+r) \times (1-s) . \tag{14}$$

Fig. 2. 4-noded (first order) quadrilateral finite element used in this study (Weaver and Johnston, 1984).

The 3x3 Jacobian matrix required in this formulation is;

$$J = \begin{bmatrix} 0 & x_r & y_r \\ 0 & x_s & y_s \\ 1 & 0 & 0 \end{bmatrix}, \tag{15}$$

where

$$x_r = \sum_{i=1}^{4}(h_{i,r}x_i)\dots\dots\dots y_r = \sum_{i=1}^{4}(h_{i,r}y_i)$$
$$x_s = \sum_{i=1}^{4}(h_{i,s}x_i)\dots\dots\dots y_s = \sum_{i=1}^{4}(h_{i,s}y_i) \tag{16}$$

The inverse of J becomes

$$J^{-1} = \begin{bmatrix} 0 & r_x & s_x \\ 0 & r_y & s_y \\ 1 & 0 & 0 \end{bmatrix}. \tag{17}$$

We need certain derivatives with respect to local co-ordinates, which are placed into a 3x3 matrix;

$$\begin{bmatrix} w_r & u_r & v_r \\ w_s & u_s & v_s \\ w_z & u_z & v_z \end{bmatrix} = \sum_{i=1}^{4} \begin{bmatrix} f_{i,r}w_i & zf_{i,r}\varphi_{xi} & -zf_{i,r}\varphi_{yi} \\ f_{i,s}w_i & zf_{i,s}\varphi_{xi} & -zf_{i,s}\varphi_{yi} \\ 0 & f_i\varphi_{xi} & -f_i\varphi_{yi} \end{bmatrix}. \tag{18}$$

Transformation of these derivatives to global coordinates is accomplished using the inverse of the Jacobian matrix, as follows;

$$\begin{bmatrix} w_x & u_x & v_x \\ w_y & u_y & v_y \\ w_z & u_z & v_z \end{bmatrix} = J^{-1}\begin{bmatrix} w_r & u_r & v_r \\ w_s & u_s & v_s \\ w_z & u_z & v_z \end{bmatrix}. \tag{19}$$

The five types of nonzero strains to be considered for this element are;

$$\varepsilon = \begin{bmatrix} \varepsilon_x \\ \varepsilon_y \\ \gamma_{xy} \\ \gamma_{xz} \\ \gamma_{yz} \end{bmatrix} = \begin{bmatrix} u_x \\ v_y \\ u_y + v_x \\ u_z + w_x \\ v_z + w_y \end{bmatrix}. \tag{20}$$

As a preliminary matter before formulating element stiffness matrix, matrix B partitioned and z factored from the upper part, as follows (Cook et al., 1989);

$$B = \begin{bmatrix} B_k \\ B_\gamma \end{bmatrix} = \begin{bmatrix} z\overline{B}_k \\ B_\gamma \end{bmatrix}, \tag{21}$$

where B_k has three rows and B_γ has two rows, then the stiffness matrix for this element is written as;

$$K = \int_V B^T E B dV = \int_V \begin{bmatrix} z\overline{B}_k^T & B_\gamma^T \end{bmatrix} \begin{bmatrix} E_k & 0 \\ 0 & E_\gamma \end{bmatrix} \begin{bmatrix} z\overline{B}_k^T \\ B_\gamma^T \end{bmatrix} dV$$
$$K = \int_V \left(z^2\overline{B}_k^T E_k \overline{B}_k\right) + \left(\overline{B}_\gamma^T E_\gamma \overline{B}_\gamma\right) dV \tag{22}$$

Integration through the thickness yields;

$$K = \int_A \left(\overline{B}_k^T \overline{E}_k \overline{B}_k + \overline{B}_\gamma^T \overline{E}_\gamma \overline{B}_\gamma\right) dA. \tag{23}$$

Thus,

$$K = \int_A \overline{B}^T \overline{E} \overline{B} dA = \int_{-1}^{1}\int_{-1}^{1} \overline{B}^T \overline{E} \overline{B}|J| drds, \tag{24}$$

which must be evaluated numerically (Hughes et al., 1977).

In this equation, $[E_k]$ is of size 3x3 and $[E_\gamma]$ is of size 2x2. $[E_k]$, and $[E_\gamma]$ can be written as follows (Bathe, 1996; Weaver and Johnston, 1984):

$$[E_k] = \frac{t^3}{12}\begin{bmatrix} \dfrac{E}{(1-v^2)} & \dfrac{vE}{(1-v^2)} & 0 \\ \dfrac{vE}{(1-v^2)} & \dfrac{E}{(1-v^2)} & 0 \\ 0 & 0 & \dfrac{E}{2(1-v)} \end{bmatrix},$$

$$[E_\gamma] = kt\begin{bmatrix} \dfrac{E}{2.4(1+v)} & 0 \\ 0 & \dfrac{E}{2.4(1+v)} \end{bmatrix}, \qquad (25)$$

where E, v, and t are modulus of the elasticity, Poisson's ratio, and the thickness of the plate, respectively, k is a constant to account for the actual non-uniformity of the shearing stresses. By assembling the element stiffness matrices obtained, the system stiffness matrix is obtained.

2.2. Evaluation of the mass matrix

The formula for the consistent mass matrix of the plate may be written as

$$M = \int_\Omega H_i^T \mu H_i d\Omega . \qquad (26)$$

In this equation, μ is the mass density matrix of the form (Tedesco et al., 1999).

$$\mu = \begin{bmatrix} m_1 & 0 & 0 \\ 0 & m_2 & 0 \\ 0 & 0 & m_3 \end{bmatrix}, \qquad (27)$$

where $m_1 = \rho_p t$, $m_2 = m_3 = \frac{1}{12}(\rho_p t^3)$, and ρ_p is the mass densities of the plate. And H_i can be written as follows,

$$H_i = [dh_i/dx \quad dh_i/dy \quad h_i] \qquad i = 1 \dots 17. \qquad (28)$$

It should be noted that the rotation inertia terms are not taken into account. By assembling the element mass matrices obtained, the system mass matrix is obtained.

2.3. Evaluation of the frequency of plate

The formulation of lateral displacement, w, can be given as motion is sinusoidal;

$$w = W \sin \omega t . \qquad (29)$$

Here ω is the circular frequency. Substitution of Eq. (29) and its second derivation into Eq. (1) gives expression as;

$$[K - \omega^2 M]\{W\} = 0 . \qquad (30)$$

Eq. (30) is obtained to calculate the circular frequency, ω, of the plate. Then natural frequency can be calculated with the formulation below;

$$F = \omega / 2\pi . \qquad (31)$$

3. Numerical Examples

3.1. Data for numerical examples

In the light of the results given in references (Özdemir et al., 2007; Özdemir, 2012), the aspect ratios, b/a, of the plate are taken to be 1, 1.5, and 2.0. The thickness/span ratios, t/a, are taken as 0.05, 0.1, and 0.2 for each aspect ratio. The shorter span length of the plate is kept constant to be 10 m. The mass density, Poisson's ratio, and the modulus of elasticity of the plate are taken to be 2.5 kN s^2/m^2, 0.2, and 2.7x10^7 kN/m^2. Shear factor k is taken to be 5/6. The subgrade reaction modulus of the Winkler-type foundation is taken to be 500 and 5000 kN/m^3.

For the sake of accuracy in the results, rather than starting with a set of a finite element mesh size, the mesh size required to obtain the desired accuracy were determined before presenting any results. This analysis was performed separately for the mesh size. It was concluded that the results have acceptable error when equally spaced 20x20 mesh size for 4-noded elements are used for a 10 m x 10 m plate. Length of the elements in the x and y directions are kept constant for different aspect ratios as in the case of square plate.

In order to illustrate that the mesh density used in this paper is enough to obtain correct results, the first six frequency parameters of the thick plate with $b/a=1$ and $t/a=0.05$ is presented in Table 1 by comparing with the result obtained SAP2000 program and the results Özgan and Daloğlu (2015). In this study Özgan and Daloğlu used 4-noded and 8-noded quadrilateral finite element with 10x10 and 5x5 mesh size. It should be noted that the results presented for MT4 element are obtained by using equally spaced 20x20 mesh size.

3.2. Results

The first six frequency parameters of thick plate resting on Winkler foundation with free edges are compared with the same thick plate modeled by Özgan and Daloğlu (2010) and SAP program and it is presented in Table1. The subgrade reaction modulus of the Winkler-type foundation for this example is taken to be 5000 kN/m^3. This thick plate is modeled with MT4 element 20x20 mesh size for $b/a=1.0$, $t/a=0.05$ ratios.

As seen from Table 1, the values of the frequency parameters of these analyses are so close. Then writers enlarged parameters of aspect ratio, b/a, thickness/span ratio, t/a, for help the researchers.

The first six frequency parameters of thick plates resting on Winkler foundation considered for different aspect ratio, b/a, thickness/smaller span ratio, t/a, are presented in Table 2 for the with free edges, in Table 3 for thick clamped plates. In order to see the effects of the changes in these parameters better on the first six frequency parameters, they are also presented in Figs. 3-4 for the thick free plates, in Figs. 5-6 for the thick clamped plates.

As seen from Table 2, and Figs. 3, and 4, the values of the first three frequency parameters for a constant value of t/a increase as the aspect ratio, b/a, increases up to the 3rd frequency parameters, but after the 3rd frequency parameter, the values of the frequency parameters for a constant value of t/a decrease as the aspect ratio, b/a, increases.

Table 1. The first five natural frequency parameters of plates for *b/a*=1 and *t/a*=0.05.

$\lambda_i = \omega^2$	Özgan and Daloğlu (2015) PBQ8(FI)	This Study MT4 (400 element)	SAP2000
1	3990.42	4061.49	4000.00
2	3990.42	4061.49	4000.00
3	4000.40	4082.22	4000.00
4	8676.00	8762.37	8619.60
5	13957.64	17776.58	13292.31
6	17252.34	20960.35	16380.24

Table 2. Effects of aspect ratio and thickness/span ratio on the first six frequency parameters of the thick free plates resting on elastic foundation.

a)   Subgrade reaction modulus *k*=500

k	b/a	t/a	λ_1	λ_2	λ_3	λ_4	λ_5	λ_6
		0.05	430	430	438	5140	14176	17357
	1.0	0.10	199	199	212	17645	41441	53335
		0.20	94	94	106	58997	130338	168555
		0.05	431	434	440	2515	3440	11923
500	1.5	0.10	201	206	214	8026	9643	40293
		0.20	94	100	107	27419	32615	128500
		0.05	432	436	440	1389	1587	6159
	2.0	0.10	202	209	215	3235	4565	20820
		0.20	94	103	107	10912	15545	69111

b)   Subgrade reaction modulus *k*=5000

k	b/a	t/a	λ_1	λ_2	λ_3	λ_4	λ_5	λ_6
		0.05	4061	4061	4082	8762	17777	20960
	1.0	0.10	2028	2028	2045	19466	43226	55118
		0.20	981	981	1024	59866	131150	169372
		0.05	4064	4072	4084	6143	7064	15539
5000	1.5	0.10	2029	2039	2048	9852	11457	42102
		0.20	981	1004	1024	28299	33479	129354
		0.05	4065	4077	4086	5023	5217	9783
	2.0	0.10	2029	2043	2048	5059	6392	22637
		0.20	981	1013	1024	11798	16428	69980

Table 3. Effects of aspect ratio and thickness/span ratio on the first six frequency parameters of the thick clamped plates resting on elastic foundation.

a)   Subgrade reaction modulus *k*=500

k	*b/a*	*t/a*	λ_1	λ_2	λ_3	λ_4	λ_5	λ_6
		0.05	36939	149205	149205	301078	472059	477466
	1.0	0.10	108466	402992	402992	787956	1126271	1156881
		0.20	283837	885712	885712	1603877	2126830	2185266
		0.05	21497	48713	123073	125433	171534	274339
500	1.5	0.10	63733	143687	338076	343965	466814	733072
		0.20	175581	371188	752882	801534	1022285	1535569
		0.05	18205	28853	55872	111646	119141	140610
	2.0	0.10	53571	86512	165072	317108	319958	382361
		0.20	148609	234915	425641	713638	760071	849653

b)   Subgrade reaction modulus *k*=5000

k	*b/a*	*t/a*	λ_1	λ_2	λ_3	λ_4	λ_5	λ_6
		0.05	40570	152816	152816	304670	475641	481049
	1.0	0.10	110264	404763	404763	789707	1138013	1158626
		0.20	284721	886575	886575	1604729	2127672	2186119
		0.05	25132	52339	126684	129048	175139	277932
5000	1.5	0.10	65537	145475	339851	345734	468578	734821
		0.20	176470	372061	753747	802393	1023142	1536418
		0.05	21842	32485	59495	115257	122757	144221
	2.0	0.10	55377	88309	166856	318876	321736	384131
		0.20	149500	235795	426509	714505	760927	850513

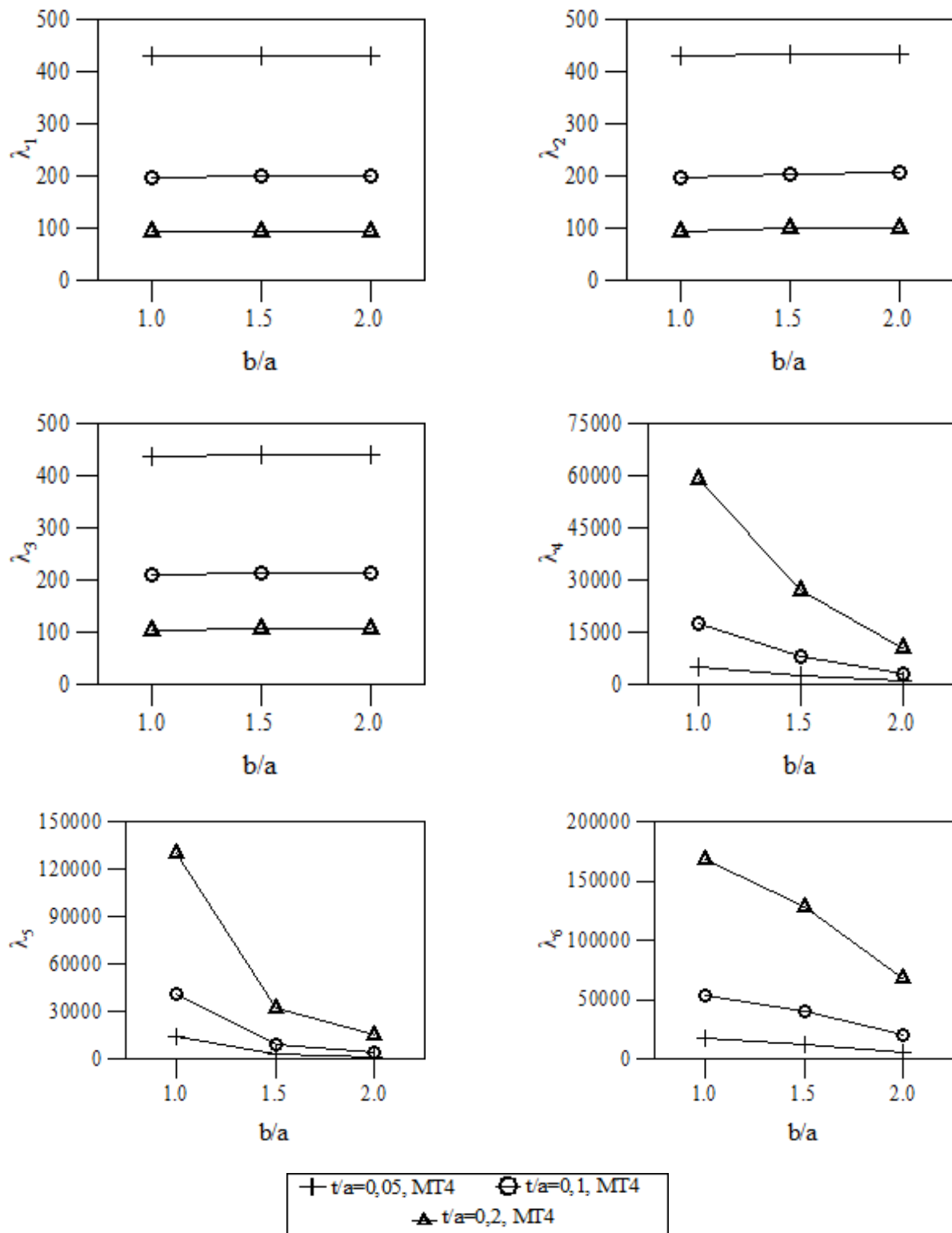In the header of each table: $\lambda = \omega^2$

Fig. 3. Effects of aspect ratio and thickness/span ratio on the first six frequency parameters of the thick free plates with subgrade reaction modulus k=500.
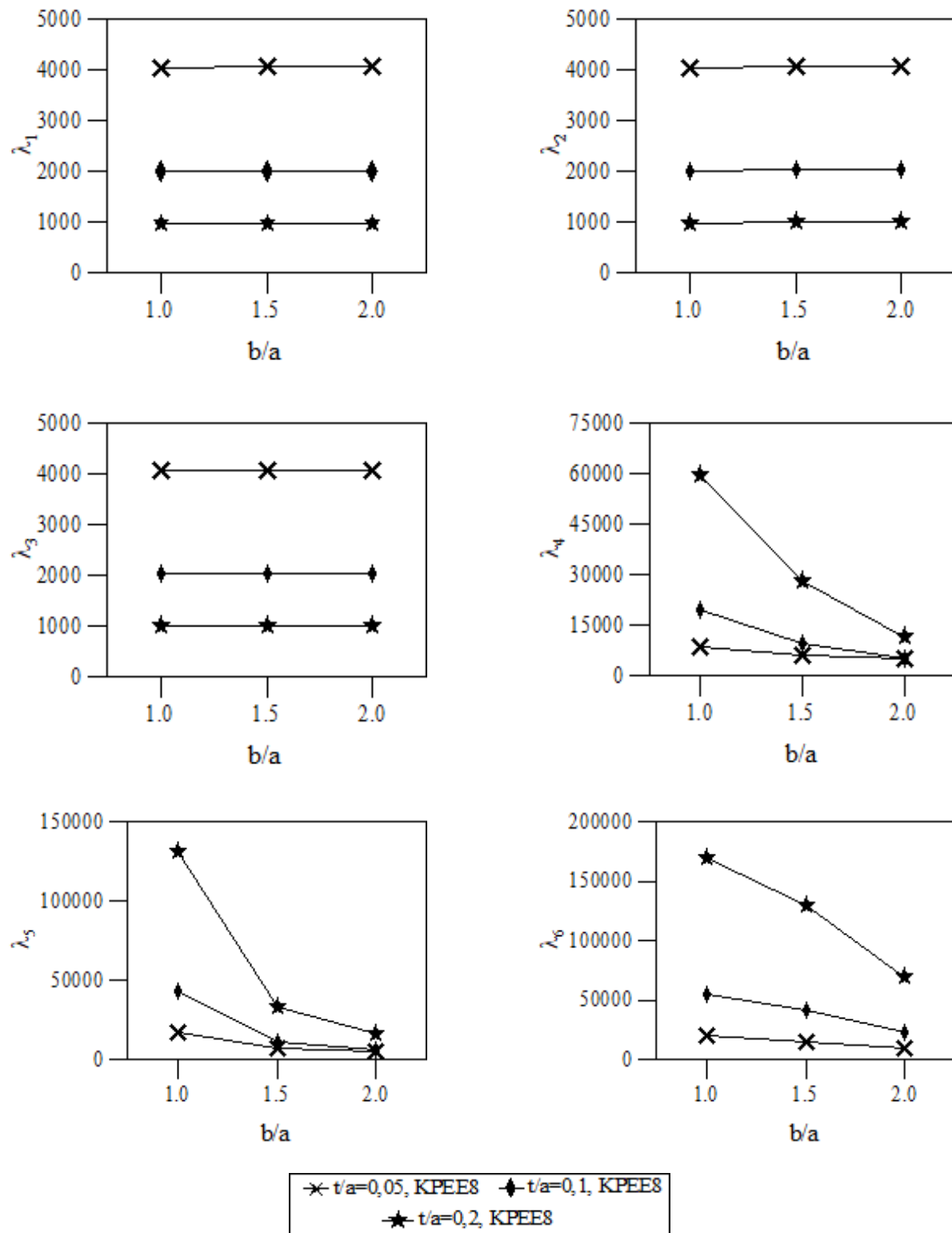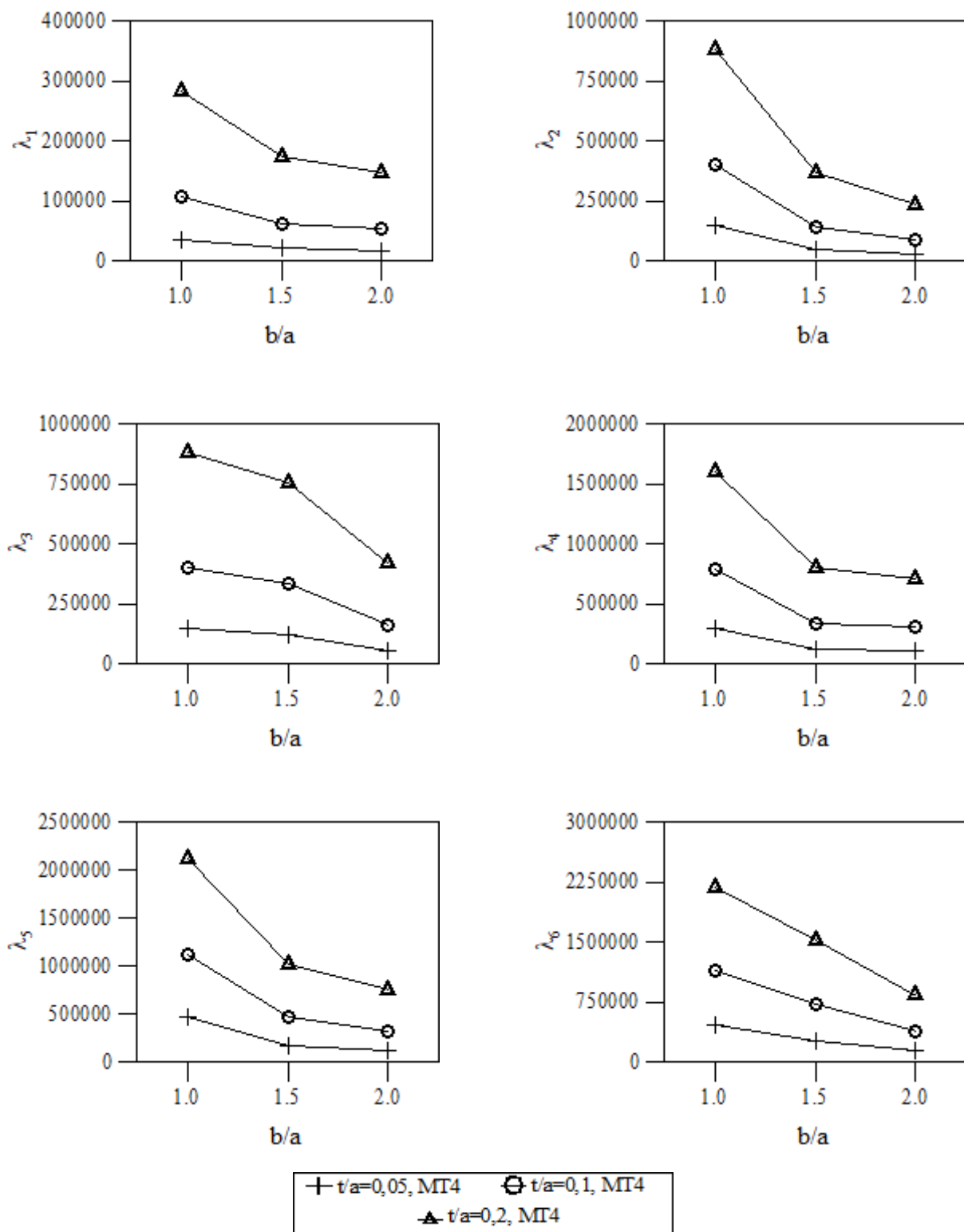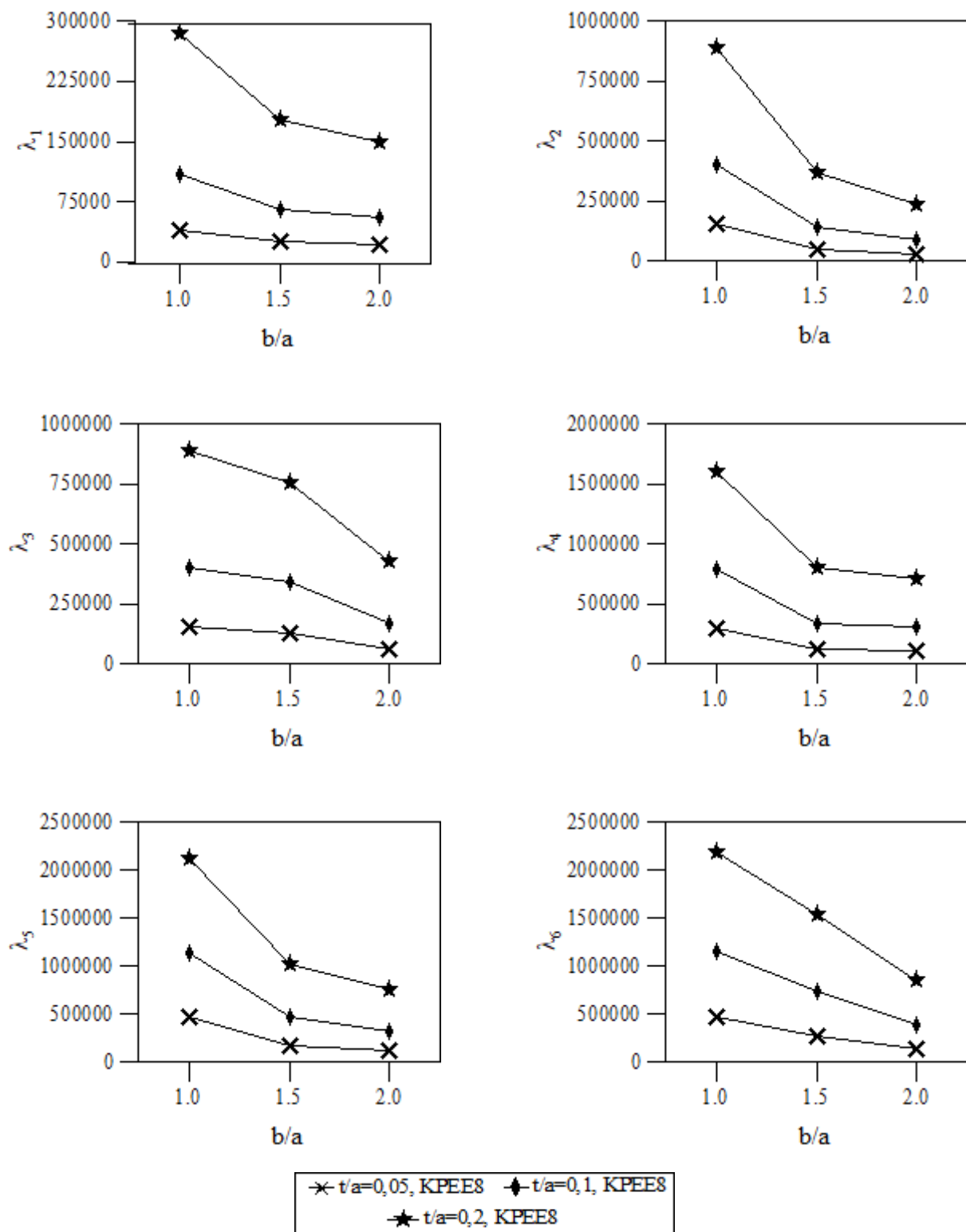
Fig. 4. Effects of aspect ratio and thickness/span ratio on the first six frequency parameters of the thick free plates with subgrade reaction modulus *k*=5000.

Fig. 5. Effects of aspect ratio and thickness/span ratio on the first six frequency parameters of the thick clamped plates with subgrade reaction modulus *k*=500.

Fig. 6. Effects of aspect ratio and thickness/span ratio on the first six frequency parameters of the thick clamped plates with subgrade reaction modulus k=5000.

As also seen from Table 2 and, Figs. 3 and 4, the values of the first three frequency parameters for a constant value of b/a decrease as the thickness/span ratio, t/a, increases up to the 3rd frequency parameters, but after the 3rd frequency parameters, the values of the frequency parameters for a constant value of b/a increase as the thickness/span ratio, t/a, increases.

The increase in the frequency parameters with increasing value of b/a for a constant t/a ratio gets less for larger values of b/a up to the 3rd frequency parameters. After the 3rd frequency parameters, the decrease in the frequency parameters with increasing value of b/a for a constant t/a ratio gets also less for larger values of b/a.

The changes in the frequency parameters with increasing value of b/a for a constant t/a ratio is larger for the smaller values of the b/a ratios. Also, the changes in the frequency parameters with increasing value of b/a for a constant t/a ratio is less than in the frequency parameters with increasing t/a ratios for a constant value of b/a.

These observations indicate that the effects of the change in the t/a ratio on the frequency parameter of the plate are generally larger than those of the change in the b/a ratios considered in this study.

As also seen from Table 2 and, Figs. 3 and 4, the curves for a constant value of b/a ratio are fairly getting closer to each other as the value of t/a increases up to the 3rd frequency parameters. This shows that the curves of the frequency parameters will almost coincide with each other when the value of the ratio of t/a increases more. After the 3rd frequency parameters, the curves for a constant value of t/a ratio are fairly getting closer to each other as the value of b/a increases. This also shows that the curves of the frequency parameters will almost coincide with each other when the value of the ratio of b/a increases more.

In other words, up to the 3rd frequency parameters, the increase in the t/a ratio will not affect the frequency parameters after a determined value of t/a. After the 3rd frequency parameters, the increase in the b/a ratio will not affect the frequency parameters after a determined value of b/a.

As seen from Table 3 and, Figs. 5 and 6, the values of the frequency parameters for a constant value of t/a decrease as the aspect ratio, b/a, increases. This behavior is understandable in that a thick plate with a larger aspect ratio becomes more flexible and has smaller frequency parameters. The decreases in the frequency parameters with increasing value of b/a ratio gets less for a constant value of t/a.

As seen from Table 3 and, Figs. 5 and 6, the values of the frequency parameters for a constant value of b/a increase as the thickness/span ratio, t/a, increases. This behavior is also understandable in that a thick plate with a larger thickness/span ratio becomes more rigid and has larger frequency parameters. The increases in the frequency parameters with increasing value of t/a ratio gets larger for a constant value of b/a.

It should be noted that the increase in the frequency parameters with increasing t/a ratios for a constant value of b/a ratio gets larger for larger values of the frequency parameters.

These observations indicate that the effects of the change in the t/a ratio on the frequency parameter of the thick plates clamped along all four edges are always larger than those of the change in the aspect ratio.

As also seen from Figs. 3, 4, 5 and 6, the curves for a constant value of the aspect ratio, b/a are fairly getting closer to each other as the value of t/a decreases. This shows that the curves of the frequency parameters will almost coincide with each other when the value of the thickness/span ratio, t/a, decreases more. In other words, the decrease in the thickness/span ratio will not affect the frequency parameters after a determined value of b/a.

In this study, the mode shapes of the thick plates are also obtained for all parameters considered. Since presentation of all of these mode shapes would take up excessive space, only the mode shapes corresponding to the six lowest frequency parameters of the thick plate free, clamped along all four edges for b/a = 1, and 2 and t/a = 0.05 are presented. These mode shapes are given in Figs. 7, 8 and 9, respectively. In order to make the visibility better, the mode shapes are plotted with exaggerated amplitudes.

As seen from these figures, the number of half wave increases as the mode number increases. It should be noted that appearances of the mode shapes not given here for the thick plates clamped along all four edges are similar to those of the mode shapes presented here.
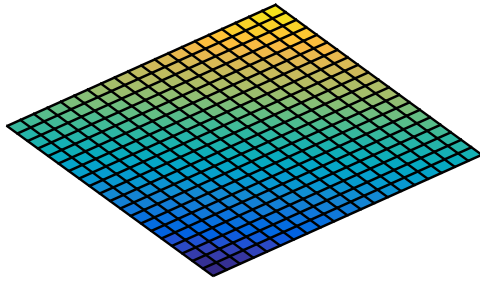
4. Conclusions

The purpose of this paper was to study parametric free vibration analysis of thick plates using first order finite elements with Mindlin's theory and to determine the effects of the thickness/span ratio, the aspect ratio and the boundary conditions on the linear responses of thick plates subjected to vibration. As a result, free vibration analyze of the thick plates were done by using first order serendipity element, and the coded program on the purpose is effectively used. In addition, the following conclusions can also be drawn from the results obtained in this study.

The frequency parameters increases with increasing b/a ratio for a constant value of t/a up to the 3rd frequency parameters, but after that the frequency parameters decreases with increasing b/a ratio for a constant value of t/a.

The frequency parameters decreases with increasing t/a ratio for a constant value of b/a up to the 3rd frequency parameters, but after that the frequency parameters increases with increasing t/a ratio for a constant value of b/a.
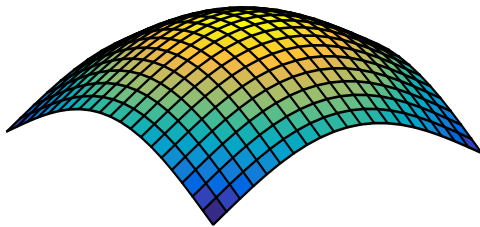
The effects of the change in the t/a ratio on the frequency parameter of the thick plate are generally larger than those of the change in the b/a ratios considered in this study.
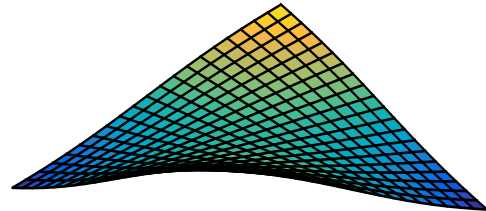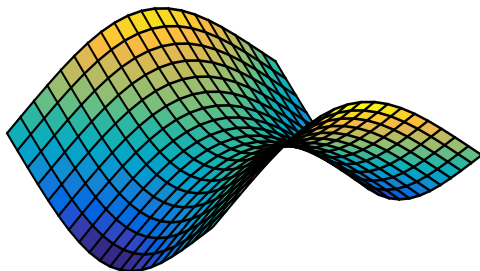
The first mode shape
(λ_1=4061)
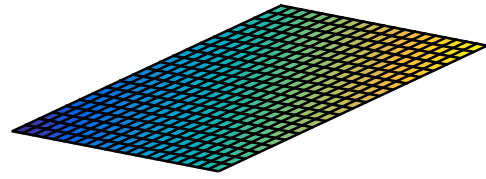
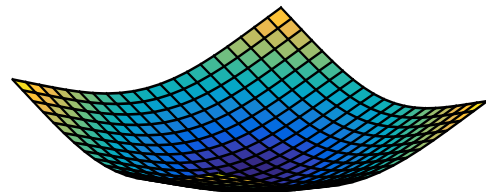The second mode shape
(λ_2=4061)

The third mode shape
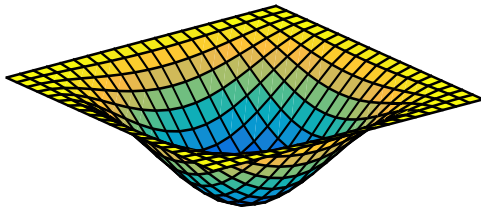(λ_3=4082)

The fourth mode shape
(λ_4=8762)

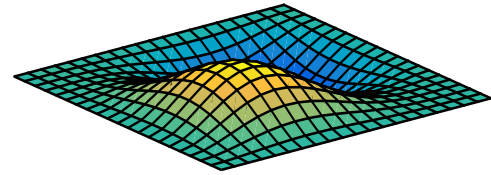The fifth mode shape
(λ_5=17777)
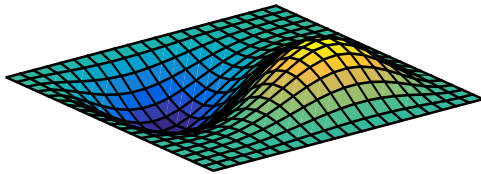
The sixth mode shape
(λ_6=20960)

Fig. 7. The first six mode shapes of the thick free plates for *b*/*a*=1.0 and *t*/*a*=0.05 with subgrade reaction modulus *k*=5000.
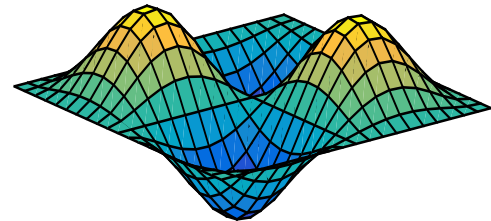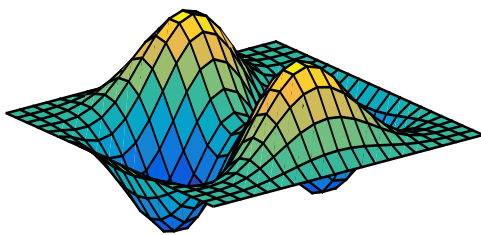
The first mode shape
$(\lambda_1=40570)$

The second mode shape
$(\lambda_2=152816)$

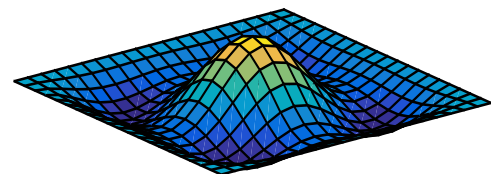The third mode shape
$(\lambda_3=152816)$

The fourth mode shape
$(\lambda_4=304670)$
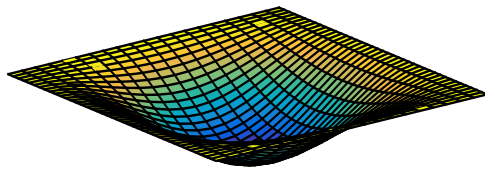
The fifth mode shape
$(\lambda_5=475641)$

The sixth mode shape
$(\lambda_6=481049)$

Fig. 8. The first six mode shapes of the thick clamped plates for b/a=1.0 and t/a=0.05 with subgrade reaction modulus k=5000.

The first mode shape
(λ_1=21842)

The second mode shape
(λ_2=32485)

The third mode shape
(λ_3=59495)

The fourth mode shape
(λ_4=115257)

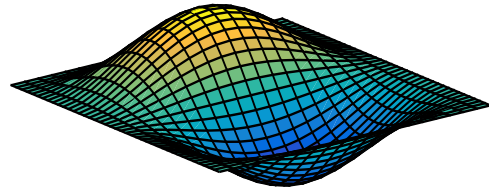The fifth mode shape
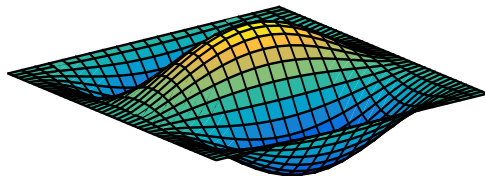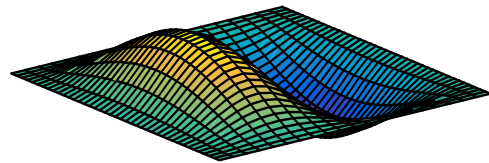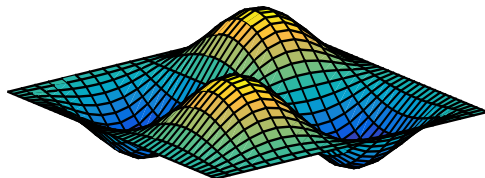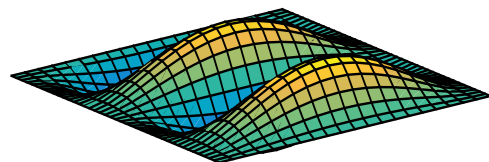(λ_5=122757)

The sixth mode shape
(λ_6=144221)

Fig. 9. The first six mode shapes of the thick clamped plates for *b/a*=2.0 and *t/a*=0.05 with subgrade reaction modulus *k*=5000.

References

Ayvaz Y, Durmuş A (1995). Earthquake analysis of simply supported reinforced concrete slabs. *Journal of Sound & Vibration,* 187(3), 531-539.

Bathe KJ (1996). Finite Element Procedures. Prentice Hall, Upper Saddle River, New Jersey.

Belounar L, Guenfound M (2005). A new rectangular finite element based on the strain approach for plate bending. *Thin-Walled Structures,* 43, 47-63.

Bergan PG, Wang X (1984). Quadrilateral plate bending elements with shear deformations. *Computers & Structures,* 19(1-2) 25-34.

Brezzi F, Marini LD (2003). A nonconforming element for the Reissner-Mindlin plate. *Computers & Structures,* 81, 515-522.

Caldersmith GW (1984). Vibrations of orthotropic rectangular plates. *ACUSTICA,* 56, 144-152.

Cen S, Long YQ, Yao ZH, Chiew SP (2006). Application of the quadrilateral area co-ordinate method: Anew element for Mindlin-Reissner plate. *International Journal of Numerical Methods in Engineering,* 66, 1-45.

Cook RD, Malkus DS, Michael EP (1989). Concepts and Applications of Finite Element Analysis. John Wiley & Sons, Inc., Canada.

Fallah A, Aghdam MM, Kargarnovin MH (2013). Free vibration analysis of moderately thick functionally graded plates on elastic foundation using the extended Kantorovich method. *Archive of Applied Mechanics,* 83(2), 177-191.

Grice RM, Pinnington RJ (2002). Analysis of the flexural vibration of a thin-plate box using a combination of finite element analysis and analytical impedances. *Journal of Sound & Vibration,* 249(3), 499-527.

Gunagpeng Z, Tianxia Z, Yaohui S (2012). Free vibration analysis of plates on Winkler elastic foundation by boundary element method. *Optical and Electronics Materials Applications II,* 529, 246-251.

Hinton E, Huang HC (1986). A family of quadrilateral Mindlin plate element with substitute shear strain fields. *Computers & Structures,* 23(3), 409-431.

Hughes TJR, Taylor RL, Kalcjai W (1977). Simple and efficient element for plate bending. *International Journal of Numerical Methods in Engineering,* 11, 1529-1543.

Jahromi HN, Aghdam MM, Fallah A (2013). Free vibration analysis of Mindlin plates partially resting on Pasternak foundation. *International Journal of Mechanics and Sciences,* 75, 1-7.

Leissa AW (1973). The free vibration of rectangular plates. *Journal of Sound & Vibration,* 31(3), 257-294.

Leissa AW (1977a). Recent research in plate vibrations, 1973–1976: classical theory, *The Shock and Vibration Digest,* 9(10), 13–24.

Leissa AW (1977b). Recent research in plate vibrations, 1973–1976: complicating effects. *The Shock and Vibration Digest,* 9(11), 21–35.

Leissa AW (1981a). Plate vibration research, 1976–1980: classical theory. *The Shock and Vibration Digest,* 13(9), 11–22.

Leissa AW (1981b). Plate vibration research, 1976–1980: complicating effects. *The Shock and Vibration Digest,* 13(10) 19–36.

Leissa AW (1987a). Plate vibration research, 1981–1985—part I: classical theory. *The Shock and Vibration Digest,* 19(2), 11–18.

Leissa AW (1987b). Plate vibration research, 1981–1985—part II: complicating effects, *The Shock and Vibration Digest,* 19(3), 10–24.

Lok TS, Cheng QH (2001). Free and forced vibration of simply supported, orthotropic sandwich panel. *Computers & Structures,* 79(3), 301-312.

Mindlin RD (1951). Influence of rotatory inertia and shear on flexural motions of isotropic, elastic plates. *Journal of Applied Mechanics (ASME),* 18(1), 31-38.

Özdemir YI (2012). Development of a higher order finite element on a Winkler foundation. *Finite Element Analysis and Design,* 48, 1400-1408.

Özdemir YI, Ayvaz Y (2009). Shear locking-free earthquake analysis of thick and thin plates using Mindlin's theory. *Structural Engineering & Mechanics,* 33(3), 373-385.

Özdemir YI, Bekiroğlu S, Ayvaz Y (2007). Shear locking-free analysis of thick plates using Mindlin's theory. *Structural Engineering & Mechanics,* 27(3), 311-331.

Özgan K, Daloğlu AT (2012). Free vibration analysis of thick plates on elastic foundations using modified Vlasov model with higher order finite elements. *International Journal of Engineering & Materials Sciences,* 19, 279-291.

Özgan K, Daloğlu AT (2015). Free vibration analysis of thick plates resting on Winkler elastic foundation. *Challenge Journal of Structural Mechanics,* 1(2), 78-83.

Özkul TA, Ture U (2004). The transition from thin plates to moderately thick plates by using finite element analysis and the shear locking problem. *Thin-Walled Structures,* 42, 1405-1430.

Providakis CP, Beskos DE (1989a). Free and forced vibrations of plates by boundary elements. *Computer Methods in Applied Mechanical Engineering,* 74, 231-250.

Providakis CP, Beskos DE (1989b). Free and forced vibrations of plates by boundary and interior elements. *International Journal of Numerical Methods in Engineering,* 28, 1977-1994.

Qian LF, Batra RC, Chen LM (2003). Free and forced vibration of thick rectangular plates using higher-order shear and normal deformable plate theory and meshless Petrov-Galerkin (MLPG) method. *Computer Modeling Engineering & Sciences,* 4(5), 519-534.

Raju KK, Hinton E (1980). Natural frequencies and modes of rhombic Mindlin plates. *Earthquake Engineering Structural Dynamics,* 8, 55-62.

Reissner E (1945). The effect of transverse shear deformation on the bending of elastic plates. *Journal of Applied Mechanics (ASME),* 12, A69-A77.

Reissner E (1947). On bending of elastic plates. *Quarterly Applied Mathematics,* 5(1), 55-68.

Reissner E (1950). On a variational theorem in elasticity. *Journal of Mathematics and Physics,* 29, 90-95.

Sakata T, Hosokawa K (1988). Vibrations of clamped orthotropic rectangular plates. *Journal of Sound & Vibration,* 125(3), 429-439.

Shen HS, Yang J, Zhang L (2001). Free and forced vibration of Reissner-Mindlin plates with free edges resting on elastic foundation. *Journal of Sound & Vibration,* 244(2), 299-320.

Si WJ, Lam KY, Gang SW (2005). Vibration analysis of rectangular plates with one or more guided edges via bicubic B-spline method. *Shock & Vibration,* 12(5), 363-376.

Soh AK, Cen S, Long Y, Long Z (2001). A new twelve DOF quadrilateral element for analysis of thick and thin plates. *European Journal of Mechanics: A/Solids,* 20, 299-326.

Tedesco JW, McDougal WG, Ross CA (1999). Structural Dynamics. Addison Wesley Longman Inc., California.

Ugural AC (1981). Stresses in Plates and Shells. McGraw-Hill., New York.

Wanji C, Cheung YK (2000). Refined quadrilateral element based on Mindlin/Reissner plate theory. *International Journal of Numerical Methods in Engineering,* 47, 605-627.

Warburton GB (1954). The vibration of rectangular plates. *Proceeding of the Institute of Mechanical Engineers* 168, 371-384.

Weaver W, Johnston PR (1984). Finite Elements for Structural Analysis. Prentice Hall, Inc., Englewood Cliffs, New Jersey.

Woo KS, Hong CH, Basu PK, Seo CG (2003). Free vibration of skew Mindlin plates by p-version of F.E.M. *Journal of Sound & Vibration,* 268, 637-656.

Zienkiewich OC, Taylor RL, Too JM (1971). Reduced integration technique in general analysis of plates and shells. *International Journal of Numerical Methods in Engineering,* 3, 275-290.

Review

Structural features of cold-formed steel profiles

Osman Tunca [a,*], Ferhat Erdal [b], Arif Emre Sağsöz [c], Serdar Çarbaş [a]

[a] *Department of Civil Engineering, Karamanoğlu Mehmetbey University, 70100 Karaman, Turkey*
[b] *Department of Civil Engineering, Akdeniz University, 07058 Antalya, Turkey*
[c] *Department of Civil Engineering, Pasinler Vocational School, Atatürk University, 25300 Erzurum, Turkey*

ABSTRACT

Using capacity of cold-formed steel sections increases thanks to the opportunities which are offered by the developing technology. Low production cost and variety of profiles that can be produce easy, fast, high quality provide to improve its popularity as a structural material. In production, Sulphur and Phosphorous accumulation region occurs at intersection region of flanges and web of hot rolled steel profile. This causes to decrease strength of profile. Other difference between cold-formed and hot rolled steel sections is that mechanical properties of steel material homogeneously distributes throughout the profile. Both in frame and truss systems, cold-formed steel profiles develop both as main and secondary bearing element. These present variety options to the designers with pure, galvanized, aluminized applications. As with many building materials, mechanical behavior of cold-formed steel profile is quite complex due to the nature of thin walled steel sections. Design and analysis methods of cold-formed steel profile are rapidly shaped day by day. The general theory of beams investigated in past studies make possible analyses of cold-formed steel profile. Moreover, in structural systems, using of cold-formed steel profile provide height strength besides sustainable, environmentalist, green building because it requires less material and cost. Although these profiles have many advantages, use of cold-formed steel profiles in our country structures is rather limited unfortunately. New steel construction regulations in Turkey also do not mention cold-formed thin walled steel structure. Main purpose of this study reviews structural specifications of cold-formed steel profiles which are applied world-wide.

ARTICLE INFO

1. Introduction

Nowadays, reinforced concrete is most commonly structural material in worldwide. Some advantageous properties of reinforced concrete such as to be poured in desired shape, to have enough number of technical personal in market, to be easily accessible provide that this material is popular. Although this material has various properties, strength-weight ratio of reinforced concrete is quietly low when it is compared with other materials. This is so important especially in long span structure. In this type of structures, steel material distinguishes with high strength-weight ratio. That steel structure can be quickly built, which

made it remarkable after WWII (World War II). With the increase in usage of steel as a structural member has expanded since the WWII. When using of this material is increase, their design criteria are developed day by day. Thus, new shaped profiles are emerged (Çiftçioğlu et al., 2017). Steel profiles are commonly produced in the market in two forms; hot rolled sections and cold formed sections. Hot rolled steel sections are generally used as structural member in long span structure and tall compression elements. However, generally, buckling capacity of cold-formed steel profiles is low. Therefore, cold-formed steel profile is assumed as economic for low-rise buildings when span is not enormous.

Cold-formed steel profiles are used as structural member in many parts of the real-world designs. As an independent building system, structures built with these type elements are implemented at mass production of two story buildings, small commercial buildings, industrial units and single-story sports hall. This structural system can be combined with other structural systems such as reinforced concrete wall and, in this way, it can be applied as a composite bearing system (Azizian, 2015). Cold-formed steel sections are made by bending a thin plate normally having a thickness starting from 1 mm. Generally, it made as structural element which has thickness from 2 mm to 6.4 mm in a certain shape. One of the advantages of cold-formed steel profile is that strength-weight ratio is much higher than hot rolled profiles. Thus, using of this structural member decreases total structural weight. For his reason, cold-formed steel structural elements are assumed as economic for low-rise and low span buildings. However, the calculations and designs of building made of cold-formed steel profiles are difficult due to complicated mechanical behaviors. Nowadays, optimization is used as an effective solution tool to design such complex problems in engineering applications (Akpınar et al., 2017). It is possible to produce cold-formed profiles in designed shape by means of developing technology. Production of cold-formed steel profile can be divined in two main processes as production of plane and bending of this plane. Industrial standard thickness is typically between 0.5 mm to 7 mm for both production methods. Steel used to produce cold-formed steel profiles has yield strength between 250 MPa and 550 MPa (Hancock, 1997).

2. General Material Properties of Cold-Formed Steel Profiles

Nonlinearity of a material can be defined as nonlinear relation between stress and strain. In other words, stress is a nonlinear function of strain. The theory of plasticity patterns mechanical reaction of material because of that material subject to deformation which cannot be repaired. Theory of plasticity presents mathematical relations which characterize elastoplastic reaction of materials. In rate independent plasticity theory, there are three main parts. These are yield criteria, yielding rule, strain hardening rule. Material nonlinearities of cold-formed steel profiles is created by considering a plastic material which has Von Mises yielding criteria and excellent flexibility. Cold forming process reveals cold forming in sections and particularly in corners of sections. As a result, yield stress increase and ductility decrease in corner regions of the sections. Material at corner regions can be anisotropic. Moreover, it can contain permanent stress. By evaluating experimental data, determining of the mechanical properties is so hard. Therefore, same material properties for all the materials are considered to simplify the model (Jegan and Prasath, 2016).

Strength of a structural member which is collapsed by buckling is related not only to yield strength but also to the modulus of elasticity (E) and tangent module (E_t).

Modulus of elasticity is defined as the slope of linear region of strain-stress curve of material. Measured value of modulus of elasticity according to standard method is between 200 GPa and 207 GPa. This value has been used as 203 GPa for cold-formed steel elements by American Iron and Steel Institute (AISI, 2007) for design purpose since 1946. There is it currently in North American Specifications. Tangent modulus is defined by slope of any point on the strain-stress curve. Tangent modulus value increase until it is equal to modulus of elasticity for absolute yielding. Tangent modulus is equal to modulus of elasticity in gradual yielding. Yet in this case, it increases until it will receive proportional limit value. When the stress proportional limit is exceeded, tangent modulus is gradually smaller than initial modulus of elasticity. Thus, steels with sharp yield stress for average slenderness have greater buckling strength than steels which has graded tensile strength. Various buckling conditions in North America Specifications are written for situation that steels maximum yielding stress is not approximately %70 less than the ones having graded yielding (AISI Standard, 2016).

Definition of shear modulus (G) is a ratio between shear stress and shear strain. Shear modulus is linear part of the slope of shear strength-strain curve. It is calculated by a traditional equation which is depended on poison ratio and modulus of elasticity ($G=E/[2*(1+\mu)]$). In this equation, if modulus of elasticity is 203 GPa and poison ratio is 0.3, shear modulus will be calculated as 78 GPa. Therefore, value of shear modulus in North America Specification is obtained (AISI, 2007; AISI Standard, 2016). This value is used in order to calculate torsional buckling stress in design of wall stud.

3. Advantages of Cold-Formed Steel Profiles

Cold-forming process has effect of increasing the yielding stress of steels. This increasing is result of that the cold forming process is well incorporated into the strain hardening range. Therefore, effect of cold forming process enhances average yielding stress between %15 and %30. It can be assumed that yielding stress increases minimum %15 for design purposes (Yu and La Boube, 2010).

There are some different properties of cold-formed profile from hot rolled profile.
i)   Cross sections of cold-formed steel profiles are designed to eliminate tolerance. These can be repeated continuously if necessary.
ii) Cold forming can be used to produce any desired shape in any desired length.
iii) Pre-galvanized or pre-coated metals can be produced. Thus, an attractive surface coating and high corrosion resistance can be obtained.
iv) All traditional connections method can be used (riveting, screwing, welding and using adhesive).
v)   High strength ratio is obtained from cold-formed product.
vi) These are generally light. Therefore, transportation and montage of cold-formed steel profiles are easy. Otherwise, this present environmentalist and

sustainable structuring because of them can be completely recycled.

vii) To send away material is possible in order to increase maximum load carrying capacity especially in beams (Narayanan et al., 2011).

Cold-formed steel profiles have not only above main advantages, but also other advantages. Decreasing weight of steel in general applications provides profit in both cost of steel and cost of transportation and montage. This is one of the main causes that provide a huge advantageous to steel profiles becoming popular nowadays. Consequently, the use of cold-formed steel is increasing day by day. Additionally, cold-formed steel can be protected against corrosion by using suitable galvanizing or powder paint. A desired thickness limitation can also be applied for components such as lipped channel profiles.

Typical cross section properties of hot rolled and cold-formed channel sections are shown in Fig. 1. When Fig. 1 is considered, by decreasing wall thickness, corresponding values of the moment of inertia (I_{xx} and I_{yy}) can be larger. Therefore, it is able to resist larger bending moments (Narayanan et al., 2011). Yet, that special care should be taken to discharge the appropriate design conditions into account for the expected buckling problems has not been ignored.
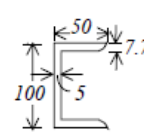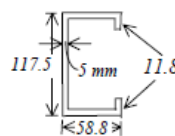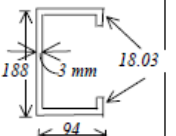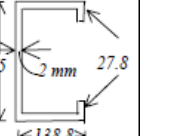
	Hot rolled channel	Cold rolled channel	Cold rolled channel	Cold rolled channel
A	$1193 \, mm^2$	$1193 \, mm^2$	$1193 \, mm^2$	$1193 \, mm^2$
I_{xx}	$1.9 \times 10^6 \, mm^4$	$2.55 \times 10^6 \, mm^4$	$6.99 \times 10^6 \, mm^4$	$15.53 \times 10^6 \, mm^4$
Z_{xx}	$38 \times 10^3 \, mm^3$	$43.4 \times 10^3 \, mm^3$	$74.3 \times 10^3 \, mm^3$	$112 \times 10^3 \, mm^3$
I_{yy}	$0.299 \times 10^6 \, mm^4$	$0.47 \times 10^6 \, mm^4$	$1.39 \times 10^6 \, mm^4$	$3.16 \times 10^6 \, mm^4$
Z_{yy}	$9.1 \times 10^3 \, mm^3$	$11.9 \times 10^3 \, mm^3$	$22 \times 10^3 \, mm^3$	$33.4 \times 10^3 \, mm^3$

Fig. 1. The geometrical properties of some channel profiles.

4. Types and Application Areas of Cold-Formed Steel Profile

Cold-formed steel elements are commonly used as C sections, Z sections and various hat channels in North America. These standard sections have traditionally been used for years. Cold-formed special section profiles are used in storage space, existing rack structural systems. Especially in the past decade, with the advantages of developing production technology and lowering the costs in mass production, new generation sections have begun to emerge. Many steel building companies start developing new generation cold-formed steel profile sections. These have larger flange, thinner web and intermediate stiffeners. Steel building companies introduce also several variations of C section profiles. Among these, the most popular sections are stiffened and web opening profiles. Thanks to these openings, both beauties are attended to the design element architecturally and the electricity, water and sewerage systems used in the structure is passed through the web openings and the assemblies are provided without damaging the structure. These cold-formed steel structures, which are designed using closed tube sections, have a higher load carrying capacity than hot rolled steel construction elements. In addition, constructions which are designed using cold-formed steel profiles generally enter the green building categories. They have great advantages in terms of material savings and therefore cost savings. Thanks to developing production technologies and analysis methods, these profiles are becoming more and more advantageous day by day (Hancock et al., 2001).

4.1. Application areas of cold-formed profiles

Cold-formed steel profiles are used as load-carrying elements in three main sections, in frames, in metal structures, and in rack systems used in industrial structure (Ghersi et al., 2005; Schafer, 2011).

4.1.1. Frames

By taking into account buckling conditions, most of the civil engineers consider that cold-formed steel profiles are suitable for using as low height and low span structural members. Using of low height and/or low span structural elements as bearing member is so much similar to timber structure element which is used for same purpose. Therefore, beams which are made from cold-formed steel profiles in single or two-story structures are likely to compete with wooden structures which is the types of bearing structure traditionally used in the market, and after that this competition will be exist. Most of in floor frame structures designed by using

cold-formed steel profiles at most medium heights is considered as an alternative for the frame platform. Each of these structures is separately mounted with studs

In the medium height structures which are designed by using cold-formed steel profiles, there is a need for an improved specification that can be applied in the technical direction in engineering and design phases. Despite the fact that North America and other some countries are specifically developed and implemented for frame structures, these required specifications are not still worked seriously in our country.

4.1.2. Steel buildings

The distinction between cold-formed steel framing systems and load carrying metal buildings made from cold-formed steel profiles is not perfect. Yet, metal buildings which are made from cold-formed steel profiles generally attempt to create a clear opening area indoors, while cold-formed steel frame structures may not do this. In addition, steel sheet is used to cover in cold-formed metal structures to substitute plywood, gypsum board etc. In addition, metal buildings which are made of cold-formed steel profiles are generally designed as a whole system. The frame structures which are made of paneled cold-formed steel profiles extend to the metal building in some situations. Load-bearing walls made of steel sheets also starts to spread rapidly in countries such as America, Australia, Hungary and Poland.

4.1.3. Rack structures

Rack structure systems which are used in storage areas and designed using cold-formed steel profiles are commonly and long-term used. Although building elements and connections have not changed significantly over the last five years, the understanding of behavior and the transformation of this understanding into improved designs have become very productive. Significant new tests have been experimented on girders, connections of vertical rack and base plates. Particularly, the analysis protocols with the use of second-order analysis and the experimental protocols have been developed and formalized. Current concerns such as the impact forces (Gilbert and Rasmussen, 2011a, 2011b) and gradual collapse (Ng et al., 2009) are seemed to have found their place in recent studies. Standard (specification) organizations that support the industry of rack systems which are made from cold-formed steel profiles are quite effective. In many cases, these are highly developed due to their complex nature of rack structural performance. For example, the Australian-based rack standard (AS 4084, 2012) provides fully coded guidance in the performance of geometric and material nonlinear analyzes on faulty structures.

5. Conclusions

The general material properties of cold-formed steel profiles, advantages over hot-rolled structural elements, partial mechanical properties, type of cross-section shapes and using areas of these steel profiles are shortly reviewed in this study. Cold-formed steel profiles are used in a wide range as the main load bearing element and / or the secondary element in many important buildings. The using areas of these profiles are expanding day by day. New analysis and design methods accelerate the success and spreading of cold-formed steel profiles. Looking at the development of cold-formed steel profiles from past to present, it is possible to say that the development and application potential of these new generation structural elements continues to increase.

Today, the construction industry has an important negative impact on the environment from the start of raw materials collection, transportation, manufacturing to the completion of the construction of buildings. Buildings of structure do not only produce more waste, but also cause more consumption by requiring transport and electricity (emissions) and generally cause landscaping damage, ecological degradation, destroyed natural habitats and forests. For this reason, a variety of technologies are currently being employed for construction systems that are ungenerous for the consumption of energy resources, as well as easy to build, comfortable, more safety and cost saving construction systems. Herein, using of cold-formed steel profiles in structural systems provides environmental construction because they require less material to bear the same load than other types of materials and reduce the amount of waste material on construction sites. In addition, using of cold-formed steel profiles reduces amount of waste materials which emerged in the construction site due to the fact that structure members and panels can be produced in workshops, factories and then it is transported to the construction site and it is mounted.

Most important advantages of cold-formed steel profiles are that it is necessary to have the possibility of forming sections in different shapes in order to obtain income of maximum resistance in the sections which are made from these profiles, to be light, to have high strength and rigidity, to have high accuracy and fast and easy installation in application detail. It has been found that the weight of a structure which is built by using cold-formed steel profiles is about 573% lighter than a building system made of reinforced concrete elements and about 59% less than a building system made by using steel elements.

REFERENCES

AISI (2007). Cold-Formed Steel Design Manual. American Iron and Steel Institute.

AISI (2016). North American Specification for the Design of Cold-Formed Steel Structural Members. American Iron and Steel Institute

Akpınar ME, Yıldızel SA, Karabulut Y, Doğan E (2017). Simulation optimization for transportation system: A real case application. *TEM Journal*, 6(1), 97-102.

AS4084 (2012) Steel Storage Racking. Australian Standard.

Azizian H (2015). Constructional system of cold-formed light steel framing (LSF). *Cumhuriyet University, Faculty of Science, Science Journal (CSJ)*, 36(3), 2135-2142.

Çiftçioğlu AÖ, Yıldızel SA, Yildirim MS, Doğan E (2017). Wind load design of hangar-type closed steel structures with different roof pitches using Abaqus CAE software. *TEM Journal*, 6(2), 336-341.

Ghersi A, Landolfo R, Mazzolani FM (2005). Design of Metallic Cold-Formed Thin-Walled Members. Spon Press.

Gilbert BP, Rasmussen KJR (2011a). Impact tests and parametric impact studies on drive-in steel storage racks. *Engineering Structures*, 33(5), 1410–1422.

Gilbert BP, Rasmussen KJR (2011b). Determination of accidental forklift truck impact forces on drive-in steel rack structures. *Engineering Structures*, 33(5), 1403–1409.

Hancock GJ (1997). Light gauge construction. *Progress in Structural Engineering and Materials*, 1(1), 25–30.

Hancock GJ, Murray TM, Ellifritt DD (2001). Cold-formed steel structures to the AISI specification, Marcel Dekker.

Jegan J, Prasath J (2016). Behaviour of built-up cold-formed steel sections. *International Journal of Advanced Engineering Research and Technology*, 4(4), 83-86.

Narayanan R, Kalyanaraman V, Santhakumar AR, Seetharaman S, Satish Kumar SR, Arul Jayachandran S, Senthil R (2011). Teaching Material, Institute for Steel Development & Growth.

Ng ALY, Beale RG, Godley MHR (2009). Methods of restraining progressive collapse in rack structures. *Engineering Structures*, 31(7), 1460–1468.

Schafer BW (2011). Cold-formed steel structures around the World. *Steel Construction*, 4(3), 1-9.

Yu WW, La Boube RA (2010). Cold-Formed Steel Design. John Wiley, 4th Edition.